

# Fundamentals of desiccation cracking of fine-grained soils: experimental characterisation and mechanisms identification

H. Peron, T. Hueckel, L. Laloui, and L.B. Hu

**Abstract:** This paper presents the results of a comprehensive experimental study of the desiccation of fine-grained soils. Air drying of initially saturated soil slabs in controlled conditions is investigated by performing three kinds of tests: free desiccation tests, constrained desiccation tests (prevented shrinkage), and crack pattern tests. Strains, suction, water content, and crack geometry are investigated. Results reveal that unconstrained drying exhibits two stages: a domain with large, mostly irrecoverable deformations and degree of saturation close to 100%, followed by a domain with lower deformations at a decreasing degree of saturation. Homogeneous soil macroscopic cracking is possible only in the presence of boundary constraints and (or) moisture gradients, inducing the build-up of tensile stresses. Results also show that, for the initially saturated remoulded soils tested here, in the whole sample and near a crack initiation point, the degree of saturation remains very close to 100% until cracking, while cracking onset, the air-entry suction, and the shrinkage limit are close to each other. Cavitation nuclei and the formation of an irregular drying front at cracking initiation are commented upon in light of this observation. Finally, results suggest that the crack pattern geometry is the result of energy redistribution. A quantification of the process is proposed.

*Key words:* desiccation, crack initiation, suction, air-entry value, crack pattern.

**Résumé :** Cet article présente les résultats d'une étude expérimentale complète de la dessiccation de sols fins. Le séchage de sols initialement saturés est étudié dans des conditions contrôlées et à température ambiante. Trois types d'essais ont été effectués : essais de dessiccation libre, essais de dessiccation avec contraintes (le retrait est empêché dans une direction) et essais de plans de fissures. Les déformations, la succion, la teneur en eau et la géométrie des fissures ont été investiguées. Les résultats démontrent que le séchage sans contrainte présente deux étapes : un domaine durant lequel les déformations sont grandes et irréversibles et le degré de saturation reste près de 100 %, suivi d'un domaine durant lequel les déformations sont plus faibles et le degré de saturation diminue. Pour un sol homogène, des fissures macroscopiques apparaissent seulement lorsqu'il y a des contraintes aux frontières et (ou) des gradients d'humidité, ce qui induit des contraintes en tension. Les résultats montrent aussi que pour les silts et argiles remaniés initialement saturés utilisés dans cette étude, le degré de saturation reste très près de 100 % jusqu'à la fissuration. De plus, la fissuration, l'entrée d'air et la limite de retrait sont proches les unes des autres. Suite à ces observations, l'existence de germes de cavitation et la formation d'un front de séchage irrégulier lors de l'initiation des fissures sont discutées. Finalement, les résultats suggèrent que la géométrie des fissures résulte d'une redistribution de l'énergie à travers le corps. Une quantification du processus est proposée.

*Mots-clés :* dessiccation, initiation de fissure, succion, succion à l'entrée d'air, géométrie des fissures.

## Introduction

Drying of soils and the ensuing cracking are crucial issues in geo-environmental engineering. Drying fractures strongly affect permeability and may compromise the integrity of

structures, such as clay buffers for nuclear waste isolation. In addition, soil cracking is the cause of substantial damage in foundation-supported structures. Compressibility increases substantially while the rate of consolidation decreases with the appearance of desiccation cracks (Morris et al. 1992). Cracks are also a possible precursor for inception of a failure surface at the top of dams and embankments. Assessment of the potential for such damage is difficult, as the mechanisms and principal variables in the process are not fully understood, despite decades of research and substantial progress, e.g., Corte and Higashi (1960), Abu-Hejleh (1993), Konrad and Ayad (1997a, 1997b).

Desiccation macrocracks are likely to occur if the drying shrinkage is constrained and (or) if tensile stresses are generated in the soil such that its tensile strength is reached (Corte and Higashi 1960). Typically, these constraints can arise from different causes (Hueckel 1992; Peron et al. 2009b):

Received 30 January 2008. Accepted 31 March 2009. Published on the NRC Research Press Web site at cgj.nrc.ca on 10 October 2009.

**H. Peron<sup>1</sup> and L. Laloui.** Ecole Polytechnique Fédérale de Lausanne (EPFL), Laboratory of Soil Mechanics (LMS), Station 18, CH-1015 Lausanne, Switzerland.

**T. Hueckel and L.B. Hu.<sup>2</sup>** Duke University, Department of Civil and Environmental Engineering, Durham, NC 27708, USA.

<sup>1</sup>Corresponding author (e-mail: herve.peron@epfl.ch).

<sup>2</sup>Present address: University of Vermont, Burlington, VT, USA.

- (1) A frictional or any other traction or displacement boundary condition.
- (2) Any eigen-stress concentrations within the soil sample.
- (3) Intrinsic factors, such as soil texture and soil structure.

In the field, cause (1) can arise from any restraining structure and cause (2) from soil moisture gradients, which do not respect the strain compatibility conditions (see e.g., Kowalski 2003).

This paper is focused on causes (1) and (2). It intends to identify the mechanisms of desiccation and to quantify the processes of drying shrinkage leading to cracking, by establishing experimental relationships between drying and cracking on one hand and physical variables at the macroscale on the other. The variables investigated are water content, suction, saturation degree, strains, stresses, and crack geometry. Previous research works are not numerous. Corte and Higashi (1960) conducted free-shrinkage and friction-shrinkage tests to measure strain evolutions. The main objective of their pioneering work was to estimate the total (tensile) stress at the moment when the first crack appeared. Konrad and Ayad (1997a) performed field desiccation experiments on intact clay; Miller et al. (1998) carried out a small-scale desiccation test on landfill liners. Both studies focused mainly on suction evolution during drying and crack pattern geometry, without addressing shrinkage mechanisms, and mechanical conditions of crack initiation. Kleppe and Olson (1985), Daniel and Wu (1993), and Albrecht and Benson (2001) conducted desiccation tests on compacted soils used for clay liners and covers. Their main aim was to estimate the hydraulic conductivity decay of such cracked soil specimens. Only a few empirical relationships between cracking potential, shrinkage strains, and compaction conditions have been proposed. Kodikara et al. (2000) provided a valuable report on the state of the art on existing experimental work in the general field of desiccation cracking of soils.

A paramount question that arises during an investigation of desiccation in an initially saturated soil is whether cracking occurs when the soil is still saturated. In the existing studies (Abu-Hejleh and Znidarcic 1995; Konrad and Ayad 1997a, 1997b; Lloret et al. 1998; Chertkov 2002; Nahlawi 2004, among others), it is either assumed that the soil is saturated at cracking or it is concluded that the soil is saturated at cracking based on the measurements over the whole sample or on an extended area in the field. However, to the authors' knowledge, there is no experimental evidence concerning the actual value of the degree of saturation at the onset of cracking. Related to this topic, cavitation and air entry have been suggested as fundamental mechanisms of cracking initiation in materials such as gels (Scherer 1990), but this requires clarifications when dealing with soils (Guan and Fredlund 1997). Some insight into the relationship between cracking and pore-water cavitation onset is provided by Hu et al.<sup>3</sup> Finally, it has been repeatedly noted that the desiccation crack patterns show remarkable periodicity, both in nature and in the laboratory (see e.g., Bejan 2000). Their quantification remains elusive for soils.

The present paper reports investigations of the desiccation behaviour of homogeneous cohesive soils with a focus on the mechanisms of drying shrinkage and crack initiation.

First, the experimental procedures are described for the three kinds of tests: free (unconstrained) desiccation tests, constrained desiccation tests, and crack pattern tests. Then, the experimental results are presented and their significance is discussed.

## Experimental procedures

### General experimental program

The general adopted approach to the evaluation of soil desiccation consisted of studying two limiting cases of the drying of long bar-shaped samples of fine-grained soils wetted with water: free desiccation tests, for which boundary constraints were minimized, and constrained desiccation tests, for which an axial (one-dimensional) constraint was intentionally induced, leading to the formation of a pattern of parallel cracks. The essential data to be obtained were the void ratio ( $e$ ), gravimetric water content ( $w$ ), suction ( $s$ ) in soil under drying conditions, as well as the evolution of these variables and their possible correlation to cracking.

The following measurements were carried out:

- Deformational response during both free and constrained desiccation tests. Comparison of both results provides a quantification of the process in terms of stresses and strains.
- Water content, suction, and saturation degree ( $S_r$ ) during drying and at the instant of cracking in the vicinity of each newly formed crack during constrained desiccation tests. A batch of tests was undertaken to investigate the state of saturation at cracking more fully, as well as to understand the implication of cavitation in the phenomenon, using three different soils with distinct and well-known air-entry values. The dependence of cracking suction and water content on initial water content was also investigated.
- Spacing and width of cracks during constrained desiccation tests.
- Geometrical characteristics of two-dimensional crack patterns obtained on square-shaped bars (in addition to the one-dimensional free and constrained desiccation tests).

### Material characteristics and preparation

The tested materials included Bioley silt, Sion silt, and La Frasse clay (three Swiss soils). The Bioley silt properties are: liquid limit,  $w_L = 31.8\%$ ; plastic limit,  $w_P = 16.9\%$ ; unit weight of solid particles,  $\gamma_s = 27.1 \text{ kN/m}^3$ . The Sion silt properties are:  $w_L = 25.4\%$ ;  $w_P = 16.7\%$ ;  $\gamma_s = 27.4 \text{ kN/m}^3$ . The La Frasse clay properties are:  $w_L = 30.7\%$ ;  $w_P = 20.3\%$ ;  $\gamma_s = 26.8 \text{ kN/m}^3$ . For Bioley silt, Sion silt, and La Frasse clay, all particles are smaller than  $90 \mu\text{m}$ ,  $0.5 \text{ mm}$ , and  $0.4 \text{ mm}$ , respectively. Clay minerals in Bioley silt are illite (10% of the total amount of mineral species), smectite (10%), and chlorite (5%). Clay minerals in Sion silt are illite and chlorite (about 8% of the total amount of the species).

Samples were prepared with a unique and reproducible method as follows. The dry soil powder was mixed with deaired and demineralised water at a gravimetric water content equal to 1.5 times the liquid limit. The resulting slurry was then vigorously mixed and vibrated for 2 min to remove

<sup>3</sup>Hu, L.B., Hueckel, T., Peron, H., and Laloui, L. Shrinkage of desiccating soils: a bi-modal porosity model. Submitted for publication.

air bubbles. Such a preparation guarantees an initially saturated state. After being prepared, the soil was left to settle for at least 1 day before the test to ensure homogenization. This preparation technique enables the soil to be as close as possible to a virgin mechanical and saturation state. Moreover, it prevents formation of any initial soil structures, such as particle aggregates.

### Water retention curve determination

Suction air-entry values of the materials prepared as initial slurry were deduced from their water retention curve (WRC), which was measured in a pressure-plate extractor. The degree of saturation at each applied suction stage was measured by a volume displacement method that greatly minimizes the volume measurement experimental error. The driving idea of such a measurement technique was to minimize constraints affecting the sample shrinkage during drying in the pressure-plate extractor. For this purpose, the soil samples were dried in Teflon containers within the pressure-plate extractor to avoid random and pervasive cracks and to obtain regularly shaped samples. The bias in volume measurement was drastically reduced by controlling the displaced fluid density and eliminating the primary source of potential body cracking that could generate error in the volume measurement. The average experimental error in saturation degree was decreased by a factor of three. The details of the procedure can be found in Peron et al. (2007).

The results (mean value and experimental error) are shown here in terms of degree of saturation and void ratio versus suction (see Fig. 1). The experimental relation is fitted to the Van Genuchten equation (Van Genuchten 1980). Van Genuchten fit is of practical interest if one wants to deduce the air-entry suction value. Air entry corresponds, by definition, to the onset of air invasion within the sample. Before air entry, the degree of saturation remains close to 100%. In this study, the air-entry suction value is computed from the Van Genuchten fit curve by extending the tangent of its central part up to its intersection with the axis of saturation of 1, as shown in Fig. 1. The suction value at the intersection corresponds to an abrupt drop of the degree of saturation from 1; hence, theoretically to the air entry. Bioley silt, Sion silt, and La Frasse clay have distinct air-entry suction values: 120, 55, and about 300 kPa, respectively. Those soils were selected to be used in the batch of tests intended to investigate soil-saturation state relationships with cracking.

Furthermore, the shrinkage limits of Bioley silt and Sion silt were determined using the standard ASTM D4943–02 method (ASTM 2002), where the resulting values are given in Table 1. It is emphasised that the shrinkage limit value determined from the standard test method implies that the soil abruptly stops shrinking while it is still saturated. This latter statement goes back to observations by Casagrande in 1938 (*Notes on soil mechanics – first semester*, Harvard University), reported in Holtz and Kovacs (1981), who sees the shrinkage limit as occurring in the 100% saturated material, followed in the drying process by the air entry. It is assumed that the void ratio take its final (residual) value at this time, which is then measured. Actually, the WRC reveals in the  $e$ - $s$  plane (Fig. 1) that shrinkage does not completely stop and that, at a given suction–water content, there

is a sharp decrease in the deformation rate rather than complete shrinkage cessation (which intervenes much later). This very point could be seen as a shrinkage limit, which is somewhat different from the one that stems from the standard test (see also a microstructural model by Hu et al. (2008, 2009)).

For Bioley and Sion silts, initially prepared as remoulded saturated slurries, air-entry values and shrinkage limit are close, as can be seen in Fig. 1. This observation is similar to the one of Fleureau et al. (1993) for saturated silts. In addition, Terzaghi et al. (1996) have made a similar observation. Air-entry values and shrinkage limit are given in Table 1. The shrinkage limit of La Frasse clay was not determined; thus, no conclusion can be drawn about the closeness of the shrinkage limit and air-entry value, although the WRC result suggests that the shrinkage is going on while desaturation starts.

### Free desiccation test procedure

#### *Sample preparation, general procedure, and drying conditions*

Free desiccation tests were conducted to avoid, as much as possible, any mechanical constraints at the boundaries due to cohesive–frictional effects during shrinkage. Thus, the drying took place on a Teflon support treated with a hydrophobic substance that contained silicon and ethanol. A device was designed to obtain regular and reproducible bar-shaped slurry samples (see Fig. 2). The initial slurry was poured in a 295 mm × 49 mm, 12 mm high aluminium mould, lying on the Teflon plate. To avoid adherence of soil to the mould, a Teflon strip was glued to its inner surface and was treated with a hydrophobic substance as well. This mould was able to slide along two bars and was immediately removed, allowing the preparation of several identical bars. Additionally, a few tests were made with a thinner moulded bar (295 mm long, 15 mm × 15 mm square section).

All the tests were performed in a climate chamber with controlled relative humidity and temperature. Technical limitations of the climate chamber did not allow for maintaining a perfectly constant relative humidity, and a variation of ±4% (absolute value) was usually observed, which generally occurred within a 1 h period. Nevertheless, an average relative humidity of 40% was maintained during the whole test duration. The temperature was fixed at  $19 \pm 1$  °C.

#### *Experimental program*

A list of free desiccation tests for the Bioley silt samples, which summarizes the type of measurement and indicates the initial water content of each sample, is presented in Table 2.

#### *Water content – strain evolution measurements*

The bars dedicated to water content measurements were shaped using the method described above. The bars were then put aside while still lying on the Teflon plate. The average gravimetric water content was recorded with respect to time by regularly weighing of the bar as it dried. At the same time, strains were measured on a replica bar (see below). The water content–strain curve was established using

**Fig. 1.** Water retention curves (in terms of void ratio and degree of saturation versus suction): (a) Bioley silt, (b) Sion silt, and (c) La Frasse clay.

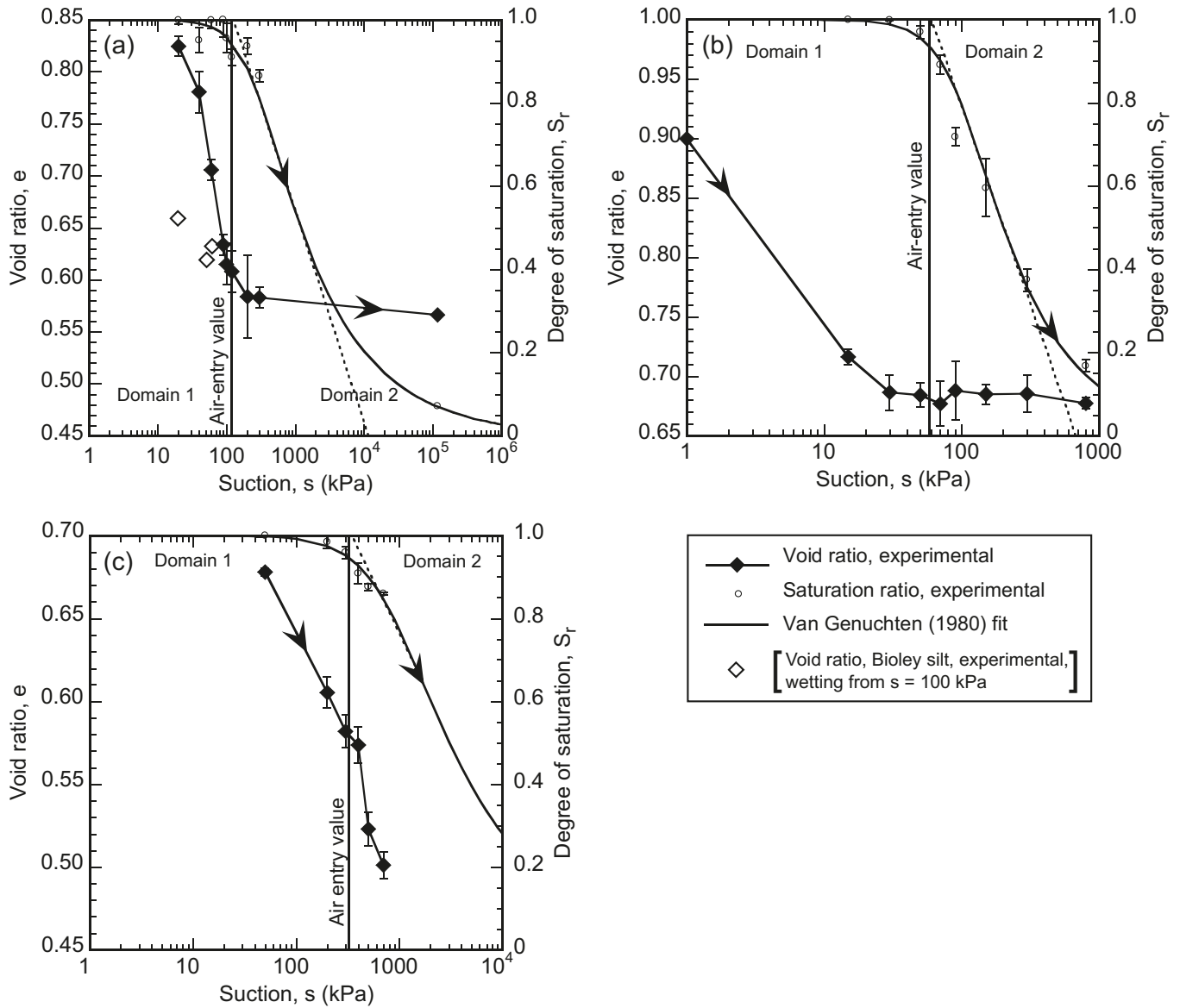


**Table 1.** Shrinkage limit and air-entry values for Bioley and Sion silts.

	Shrinkage limit		Air-entry value	
	Water content (%)	Suction (kPa)	Water content (%)	Suction (kPa)
Sion silt	24.9 (25)*	35 (35)*	24	55
Bioley silt	20.5 (22)*	200 (110)*	22.5	120

\* Number in parentheses indicates shrinkage limit values that could be deduced from the WRC.

the obtained strains evolution and corresponding water content evolution on similar bars (tests F5 to F9).

A difficulty arose in measuring strains because of the low consistency of the slurry, especially at the early stages of drying. The use of linear variable displacement transducers or strain gages turned out to be impossible. Image processing techniques or a laser with a swiping system would have

**Fig. 2.** Set up for sample fabrication.

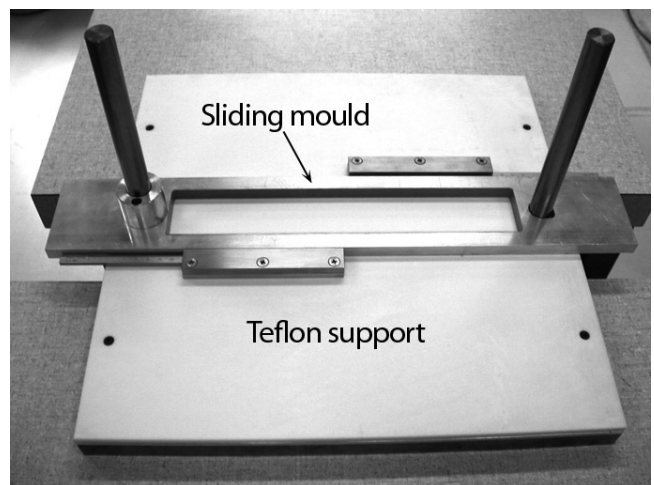


**Table 2.** Free desiccation test characteristics for Bioley silt samples.

Test No.	Initial gravimetric water content (%)	Type of measurement
F5	48.8	Average water content + axial strains
F6	48.8	Average water content + vertical strains
F7	47.8	Average water content + transverse and vertical strains
F9	48.4	Average water content + axial and vertical strains

been too heavy, considering the parallelepiped shape of the bar. Eventually, vernier calipers were selected to measure the axial and vertical strain evolution with time. The calipers were fixed on the device used for the bar fabrication, which was supporting the Teflon plate with the sample on it. The caliper accuracy was 1/50 mm. A screw point, fixed to the caliper sliding base, was regularly and carefully reset to make contact with the sample. The measurement system and a detailed view of it at the sample extremity are shown in Figs. 3a and 3b, respectively. Depending on the tests, vertical and axial strains were measured, each at two points of the bar; or transverse and axial strains were measured at two points as well, as shown in Fig. 3a; or the axial strains were simply measured at two points (at the two ends).

Axial strains in the central part of the bar were also measured (test FC1, set up shown in Fig. 4). Two thin needles were set up in the central part of the bar. Displacements of the needles embedded in the shrinking soil were controlled with the calipers in the same way as explained above. For one test (test WR), gravimetric water content distribution along the bar axis was also measured at different drying times, by rapidly retrieving fragments from several samples. In the same way, water content measurements were made for the upper and the lower parts of selected bars undergoing drying.

### Constrained desiccation test procedure

#### *Sample preparation general procedure, drying conditions*

Again, the samples were all prepared with a water content of about 1.5 times the liquid limit, using the procedure detailed above. The same procedure was used for all the tested soils (Bioley silt, Sion silt, and La Frasse clay). The bar samples were shaped the same way as for the free desiccation tests. During shrinkage, a constraint was created at the bottom surface in the longitudinal direction, by using a metal substrate with thin, 2 mm spaced parallel notches (Fig. 5). Slurry samples were prepared with the same device as for free desiccation tests, except that the Teflon plate was replaced by the notched plate. Drying was performed at the same temperature and relative humidity conditions. Cracking was invariably observed in such conditions.

#### *Experimental program*

A comprehensive list of constrained desiccation tests, which summarizes the materials used, the type of measurement, and indicates the initial water content of each test, is presented in Table 3. Note that only Bioley silt tests were used for the strain measurements; Sion silt and La Frasse clay were uniquely tested for cracking suction and saturation degree determination (see Table 3).

#### *Water content – strain evolution measurements*

As for free desiccation tests, during the constrained desiccation, total water content evolution with time was recorded by continuous weighing. At the same time, strains were measured on an identical sample. By this means, the water content–strain curve could be plotted. This was the purpose of tests CD1b and CD2. Strain measurements were not continued beyond the moment of the first crack appearance.

#### *Water content and suction measurements at the time of cracking*

In these tests, the interest was in measuring the local water content and suction in the vicinity of each newly formed crack, for various materials. To enhance the reliability of the measurements, several techniques were used. The characteristics of the totality of these tests, in particular the measured parameter, and the employed method to measure suction (tests CSW4 to CSX27) are compiled in Table 3. The procedures employed for each of them are described in detail in the following paragraphs.

#### *Water content measurements (tests CSW 4–6–12)*

In this case, as soon as a crack appeared in a bar, a small piece of the bar (about 2 cm wide) containing the crack was retrieved to measure its local water content. The remaining sample material was then used for a global water content measurement of the bar (tests CSW).

#### *Suction measurement using tensiometry (tests CSST 3–8–21)*

A number of suction measurements in the neighbourhood of each newly formed crack were performed by inserting a mini-tensiometer, UMS T5 (UMS GmbH 2001), at a small distance from the crack (tests CSST). The tensiometer was equipped with a high air-entry ceramic shaft. According to the manufacturer, this tensiometer can measure suction up to 200 kPa, without any cavitation. To ensure the validity of this domain, the ceramic cup was saturated with deaired water. The components of the probe were also filled with deaired water and connected to a vacuum pump to release the bubbles.

#### *Suction measurement using filter paper (tests CSSF 9–20)*

To increase the reliability of suction measurements, additional measurements were made using a different method, namely the filter-paper method. Filter papers were carefully calibrated and placed in contact with the newly formed crack surface, then left to equilibrate. The filter papers were calibrated beforehand by determining their water content–suction relationship. The obtained calibration curve was found to be relatively close to the available ones, especially the one generated by Al-Khafaf and Hanks (1974).

Matric suction at the time of cracking was measured by retrieving a piece of sample in the vicinity of the crack and

**Fig. 3.** Set up for strain measurements: (a) vertical and transverse strains and (b) detailed photo of the axial strain measurement system.

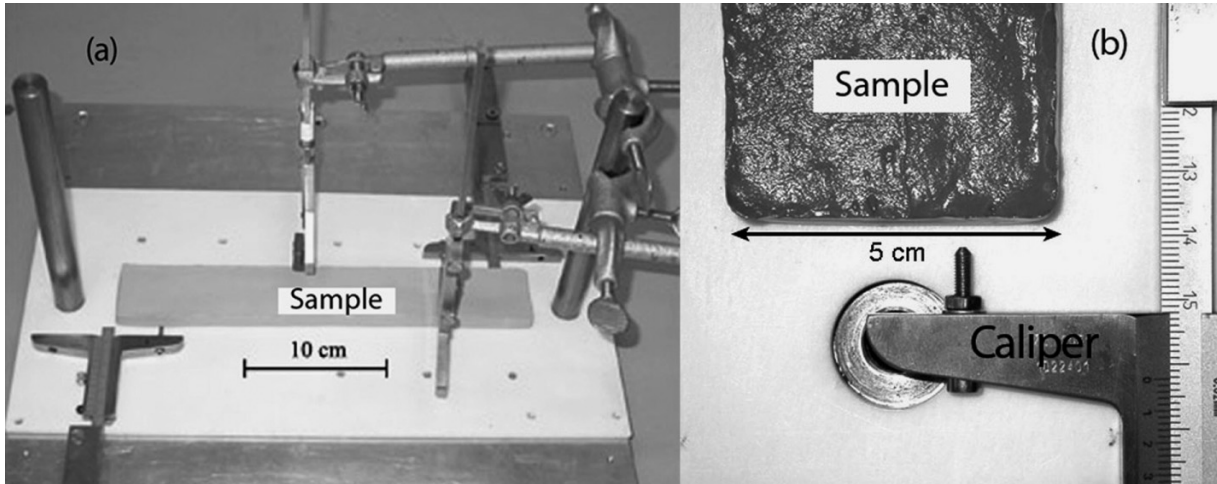


**Fig. 4.** Axial strain measurements in the central part and at the extremities of the sample (test FC1): top view.

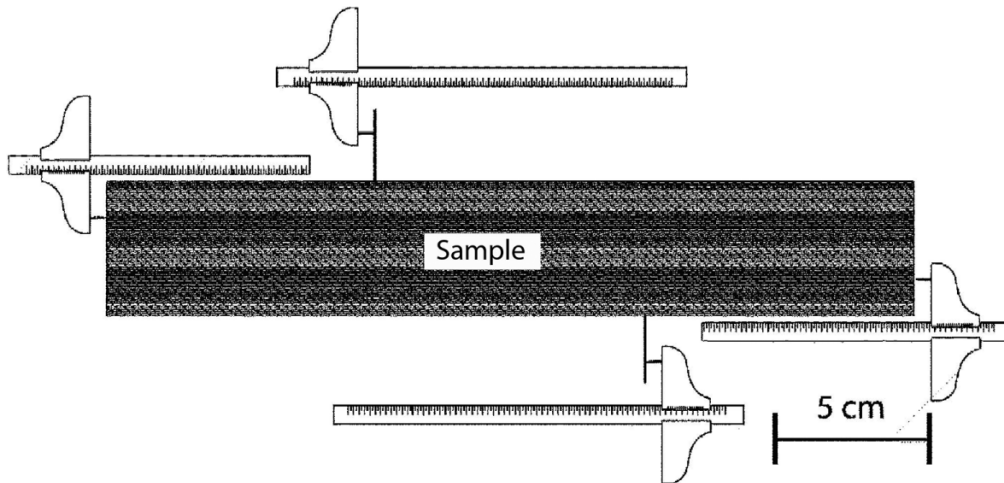
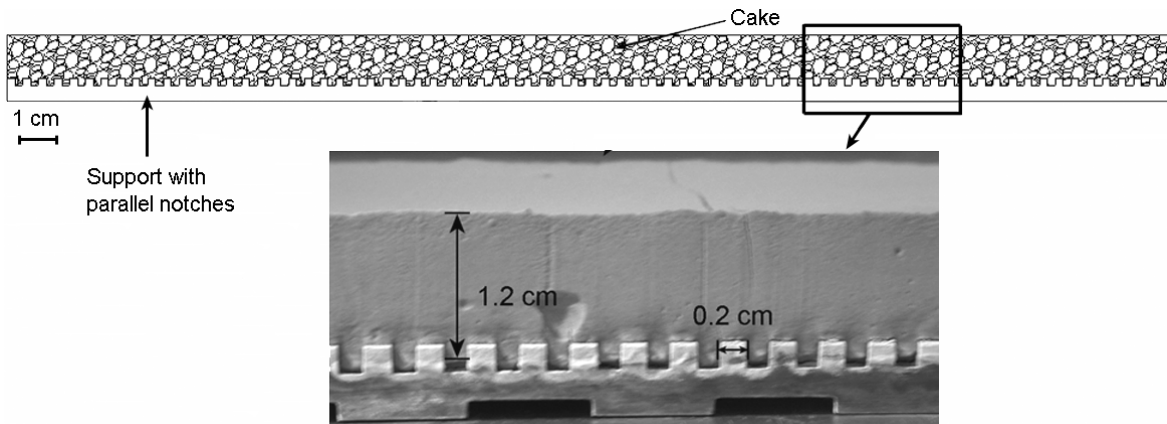


**Fig. 5.** Side view of the constrained sample lying on the notched support (scheme and magnified view).



by putting the filter paper in direct contact with the soil. The whole assembly was enveloped in a film and placed in a hermetical box. The ASTM D5298-94 standard (ASTM 1994) recommends a minimum equilibration time of 7 days. After this period, the filter paper was removed from the soil

and was weighed as rapidly as possible with a precision balance, to determine its water content. Suction was deduced from the calibration curve (in accordance with the ASTM D5298-94 standard).

To investigate the influence of the initial water content, a

**Table 3.** Constrained desiccation test characteristics.

Test No.	Initial water content (%)	Material	Type of measurement
CD1b	49.0	Bioley silt	Vertical and axial strains + water content
CD2	49.0	Bioley silt	Vertical and transverse strains + water content
CSW4	48.0	Bioley silt	Water content (for each crack)
CSW6	48.9, 45.6	Bioley silt	Water content (for each crack)
CSW12	48.5	Bioley silt	Water content (seventh crack)
CSST3	48.0	Bioley silt	Suction with tensiometer (first crack)
CSST8	46.7	Bioley silt	Suction with tensiometer (first crack)
CSST21	47.9	Bioley silt	Suction with tensiometer (seventh crack)
CSSF9	48.5	Bioley silt	Suction with filter paper (first crack)
CSSF10	48.5	Bioley silt	Suction with filter paper (first crack)
CSSF11	48.5	Bioley silt	Suction with filter paper (second crack)
CSSF12b	47.2	Bioley silt	Suction with filter paper (seventh crack)
CSSF15	47.5	Bioley silt	Suction with filter paper (seventh crack)
CSSF16	47.5	Bioley silt	Suction with filter paper (first crack)
CSSF17	47.2	Bioley silt	Suction with filter paper (first crack)
CSSF20	47.4	Bioley silt	Suction with filter paper (seventh crack)
CSI5	43.5	Bioley silt	Water content (first and second crack)
CSI7	44.4	Bioley silt	Water content (first crack)
CSII3	41.4	Bioley silt	Suction with tensiometer (first crack)
CSII9	42.2	Bioley silt	Suction with tensiometer (seventh crack)
CSX23	46.7	Sion silt	Water content (first crack)
CSX24	38.6	Sion silt	Water content (first crack)
CSX25	37.9	Sion silt	Suction with tensiometer (first crack)
CSX26	46.5	La Frasse clay	Water content (first crack)
CSX27	46.0	La Frasse clay	Water content (cracks 4, 5, 6, and 7)
CDI1	49.3	Bioley silt	Crack opening (image analysis), camera Sony XC-75/CE
CDI2	49.2	Bioley silt	Crack opening (image analysis), camera Sony XC-75/CE
CDI3	49.1	Bioley silt	Crack opening (image analysis), camera Sony XC-75/CE
CDI4	48.0	Bioley silt	Crack opening (image analysis), camera Sony XC-75/CE
CDI5	48.6	Bioley silt	Crack opening (image analysis), camera Sony XC-75/CE
CDI6	48.6	Bioley silt	Crack opening (image analysis), camera Nikon Coolpix 8800

series of tests was performed with the initial water content varying between 41% and 45% (tests CSI5–7–13–19, Table 3).

As already mentioned, Sion silt and La Frasse clay were used for water content and suction determination at cracking (tests CSX23–24–25–26–27). The characteristics of the tests are listed in Table 3; the results of the measurements are given later on, in the section entitled “Analysis of experimental results”. Water content and suction measurement techniques mentioned above were employed as well.

#### **Crack opening measurements**

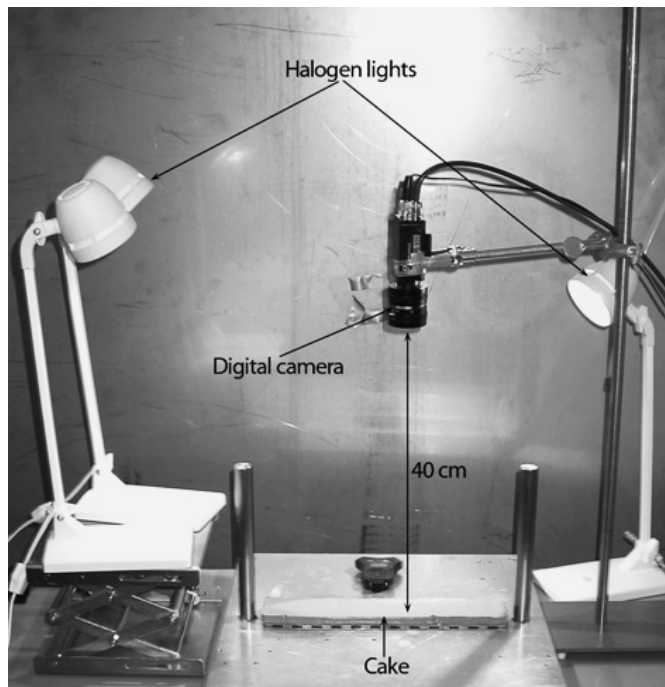
A series of bars was dedicated to crack width measurement using image analysis techniques. A digital camera was fixed at a constant distance above a sample as shown in Fig. 6. Photographs of the bar were taken periodically during cracking. Six tests were performed (CDI1 to CDI6), whose characteristics (initial water content, material, and camera used) are compiled in Table 3. For each test, the image analysis was performed using adapted software, Winanalyze version 1.4 (Micromak 1998), which uses methods of pattern recognition. In practice, film sequences (in AVI format) were built from the series of grey-level photographs taken during cracking. Such sequences were processed with

Winanalyze. The crack-opening evolution was determined by tracking the distance between two small targets at the edge of each side of an incipient crack on each frame of the film.

#### **Crack pattern test procedure**

Some constrained tests were also carried out, for which a two-dimensional restraining boundary condition was created at the bottom of square-shaped samples (30 cm × 30 cm). The principles of fabrication of the samples were exactly the same as for the constrained (and free) desiccation tests described above. In this case, the slab was lying on an aluminium plate and the constraint was created simply by the adherence between the humid sample and the plate. The constraint is thus likely to be less strong, compared with the use of the notched metallic surface. Six tests were performed (CP0 to CP5), with two different heights (slabs CP0, CP2, and CP3 of 4 mm height and slabs CP1, CP4, and CP5 of 12 mm height). All the samples were dried in the above-described humidity and temperature conditions. Only Bioley silt was tested. Some photographs of the final crack patterns were taken manually, and the geometry of the patterns in these photographs was analysed.

**Fig. 6.** Experimental set up for crack width measurement using a digital camera.



## Analysis of experimental results

### Free desiccation tests

The results of free desiccation tests (performed on the Teflon substrate) using initially water-saturated Bioley silt are presented. Tests F5 to F9 were devoted to average water content and strains evolution determination, while tests WR and FC were performed to assess moisture and strain heterogeneities, respectively.

### Water content evolution and its spatial distribution

The average gravimetric water content change with time for the F5 test is plotted in Fig. 7; similar curves were obtained for the other free desiccation tests (F6 to F9). It appears that the drying rate (i.e., slope of the gravimetric water content evolution with respect to time) is constant for about the first 2000 min. During this phase, the overall measured water mass loss due to evaporation was about 3 g/h (average value for all tests).

The evolution of the gravimetric water content distribution along the bar axis (tests WR), plotted at different drying times, is shown in Fig. 8. As the bar dries, water content heterogeneity increases for the first 14 h, before the difference between the centre and the extremities reaches 4.5%, which amounts to 10% of the initial value. Drying tends to be higher at the sample extremities than at the centre. After 14 h, the water content becomes nearly uniform at a level of 23.5%. No appreciable water content difference was revealed between the upper and lower parts of the drying sample. An additional test (also referenced as WR) was performed for comparison on a thinner bar (300 mm long, 15 mm  $\times$  15 mm square section). Results show that the water content difference between the centre and the extremities still exists, but is less pronounced (2%).

**Fig. 7.** Gravimetric average water content evolution with respect to time for free desiccation tests.

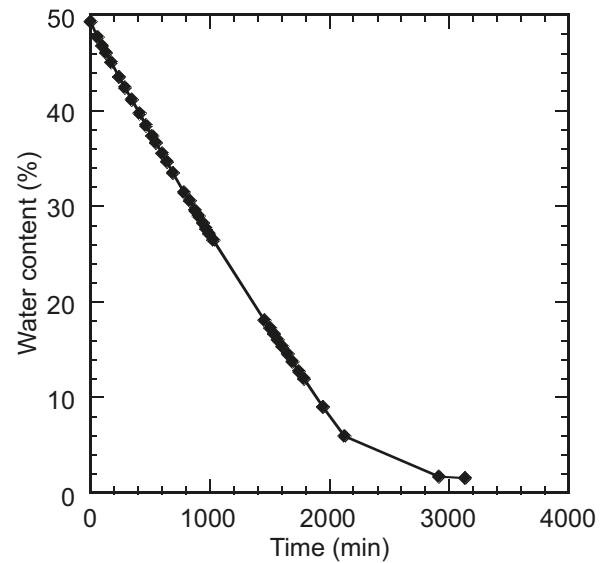
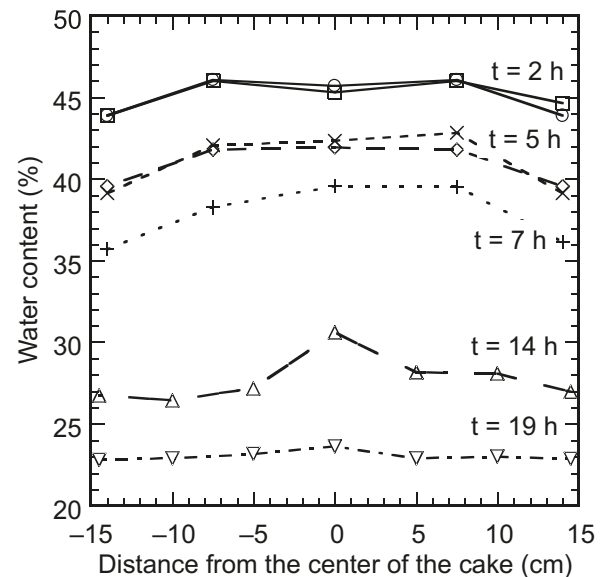


**Fig. 8.** Gravimetric water content distribution during drying (tests WR).



### Gravimetric water content – strain relationships

None of the bars in all free desiccation tests experienced cracking. Fig. 9 shows the results of the test FC; local (in the central part of the bar) and overall axial strains are plotted versus gravimetric water content. The central part of the bar shrank a bit less than its extremities, presumably because of the heterogeneity of water content, which was pointed out in Fig. 8 (the central part remained wetter).

The evolution of strains and void ratio versus overall gravimetric water content is plotted in Fig. 10 (mean values from the four tests of this type, i.e., tests F5, F6, F7, and F9, see Table 2). The void ratio standard deviation is also reported in Fig. 10 for a number of points. Actually, the use of calipers provides measurements that do not necessarily reflect the overall deformational behaviour. This is particularly true for strain measurements below  $w = 23\%$  (when

**Fig. 9.** Total and central strains versus gravimetric water content (test FC).

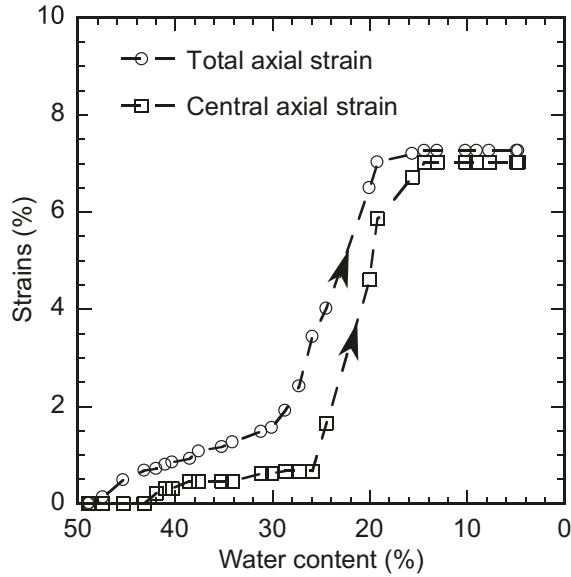
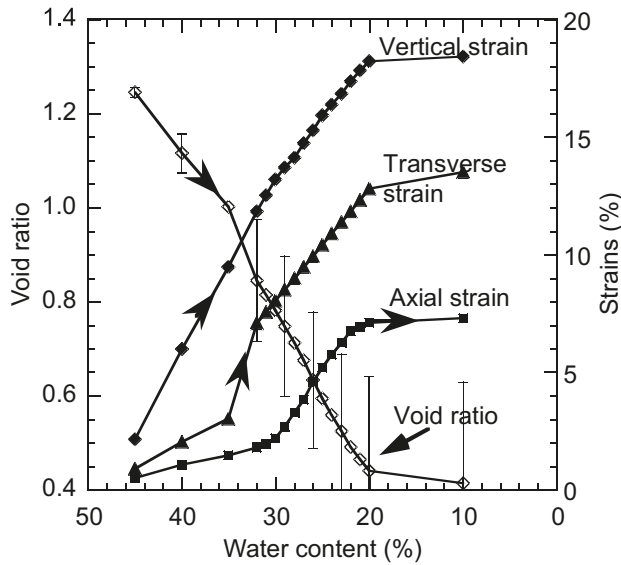


**Fig. 10.** Strains and void ratio versus average water content (tests F5, F6, F7, F9, mean values).



the samples lose their parallelepipedal shape due to curling, see below). This minimally explains the relative variability of measurements. Nevertheless, clear trends are observed in the deformational response, as discussed next.

The comparison between horizontal (i.e., both transverse and axial) and vertical strains versus gravimetric water content (Fig. 10) shows that the bar shrank more in the vertical direction than in the horizontal one, for the range of  $w > 32\%$  (which corresponds to the liquid-limit value). From this value on, the horizontal shrinkage increased noticeably. The void ratio deduced from the strains (Fig. 10) has a roughly linear evolution with water content until the value of about  $w = 20\%$ . The thinner bar experienced very similar behaviour in terms of strain and void ratio changes. Shrinkage limit of Bioley silt was determined using standard meth-

ods (see section entitled “Experimental procedures”). A value of 20.5% was found, very close to the value corresponding to the almost complete cessation of shrinkage in free desiccation tests. The shrinkage limit is also very near the air-entry value obtained from the WRC (suction equal to 120 kPa, corresponding to a water content of 22.5% (Peron et al. 2007)).

Various hypotheses may be advanced about the reasons for the disparity between horizontal and vertical strains. One possible explanation suggests that before reaching the liquid-limit value, soil is a suspension in a liquid, in which gravity-induced sedimentation and subsequent consolidation may be significant (the resulting vertical strains induce negative horizontal strain, reducing the eventual horizontal strain developed due to drying). This behaviour has been seen in slurries undergoing desiccation (Kodikara et al. 1999). In addition, Corte and Higashi (1960) observed the disparity between the vertical and horizontal strain components and attributed it to the adhesive role of the water film between the sample and the substrate, despite application of a water-repellent coating. Consequently, only the behaviour below a water content threshold of  $w = 32\%$ , corresponding to the liquid-limit value, is considered as uninhibited drying shrinkage, which is linear and isotropic. Furthermore, only shrinkage below  $w = 32\%$  was analysed. Mean values of shrinkage strains in all three directions, and considering the state at  $w = 32\%$  as a reference state, are plotted in Fig. 11.

Finally, in Fig. 12 the evolution of volumetric strains,  $\epsilon_v$ , with respect to gravimetric water content change,  $\Delta w$  ( $\Delta w = w - w_0$ , with  $w_0$  being the reference state water content; 32% here), is plotted. A linear relationship between the two variables (see also Kodikara and Choi 2006)

$$[1] \quad \epsilon_v = -\alpha \Delta w$$

yields an experimental coefficient of linear shrinkage,  $\alpha$ , equal to 1.56. Strain is positive when compressive.

Assuming the sample remains saturated in the water content range of interest and the soil skeleton is incompressible, the void ratio evolution is fully determined by the water content change. The water content change – volumetric strain relationship is then theoretically

$$[2] \quad \epsilon_v = -\frac{G_s}{1 + e_0} \Delta w = -\alpha_t \Delta w$$

where  $G_s$  is the specific gravity of the soil particles and  $\alpha_t$  is a theoretical coefficient of linear shrinkage. In eq. [2],  $e_0$  is a theoretical value of the void ratio at the reference state, assuming that soil is saturated. The theoretical value  $\alpha_t = 1.45$  obtained with  $w_0 = 32\%$  fits the experimental one deduced from Fig. 12 (eq. [1]) reasonably well.

During the tests, at and exceeding a gravimetric water content of about 23%, the bar experienced a slightly upward curling at its extremities; similar observations were made by Kodikara et al. (2004). At the very end of the drying process, the two extremities had risen about 2 mm.

**Comparison of free desiccation tests with WRC**

In Fig. 13, the void-ratio values against average gravimetric water content are shown for free desiccation tests as well as for the WRC determined with pressure-plate extractor

**Fig. 11.** Strains evolution versus water content from liquid to shrinkage limits (tests F5, F6, F7, F9, mean values).

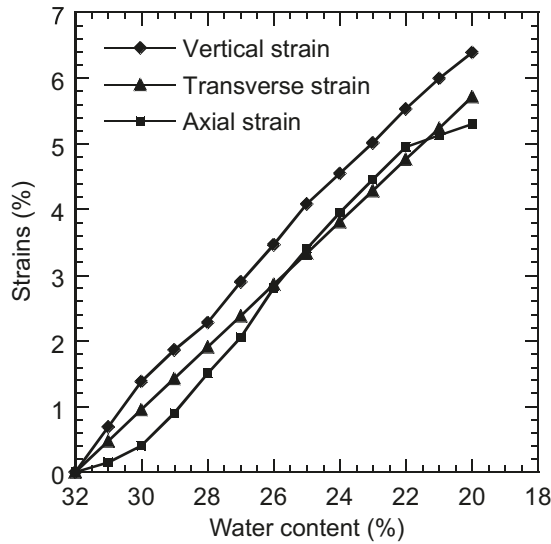
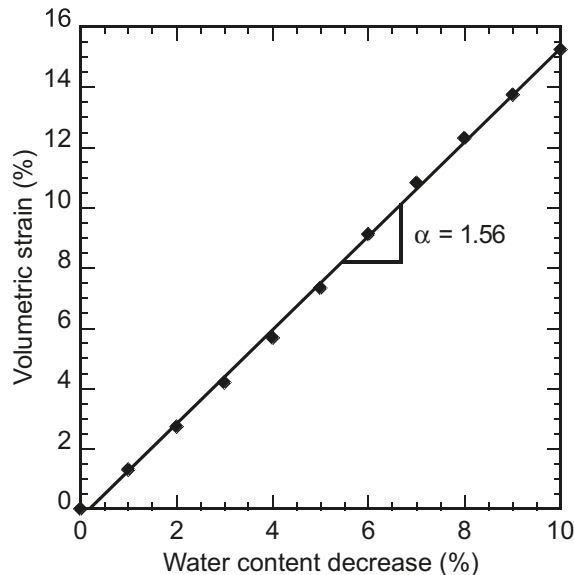


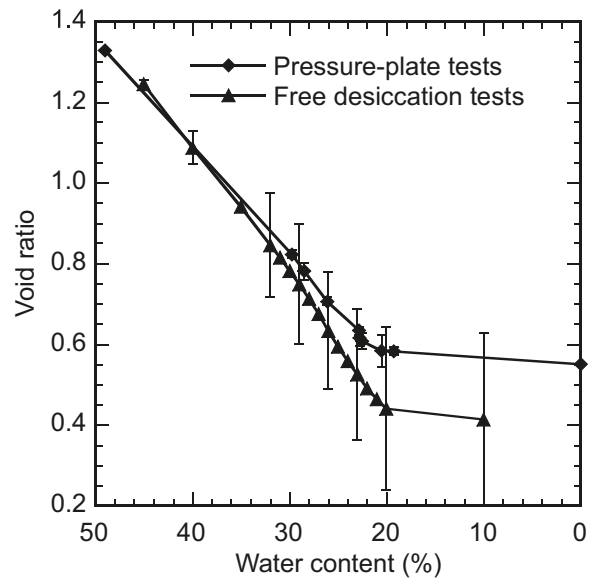
**Fig. 12.** Evolution of volumetric strain with respect to water content variation.  $\alpha$ , experimental coefficient of linear shrinkage.



tests. The standard deviation is also reported. It is clear that the pressure-plate extractor tests yield a lower uncertainty than the free desiccation tests, as seen by comparing the respective error bars in Fig. 13. In both tests, the moisture loss below 21%–23% produces almost no further shrinkage. For water content in the range between 32%–22%, a minor, but growing, departure of the free desiccation tests curve from the WRC is observed.

The comparison of the two curves allows one to address another aspect of relevance. In pressure-plate extractor tests, characteristics are determined at various equilibrium situations, once suction, strains, water content, and degree of saturation are homogeneous throughout the sample. This is not the case for the free drying slabs, in which the process is continually transient. However, as both curves (WRC and desiccation tests) reveal similar trends, the transient nature

**Fig. 13.** Comparison of free desiccation and pressure-plate extractor test results.



of the discussed desiccation tests does not seem to be relevant. From WRC results, the coefficient  $\alpha$  (eq. [1]) can also be determined by considering the strain evolution before air-entry value. By extrapolating a linear strain evolution from  $w = 30\%$ , one finds a value of  $\alpha = 1.43$ .

**General conclusions on free desiccation tests**

At this stage, it is useful to clarify the significance of the free desiccation test results. Free desiccation tests indicate that for the tested material, essentially, most of the deformations occur before the suction air-entry value, which is at a degree of saturation equal to 100%. This is in agreement with classical statements by Terzaghi (1927) and by Casagrande in 1938 (reported in Holtz and Kovacs 1981). The second stage of drying occurs at a decreasing degree of saturation and much lower deformation rates. Deformations of the first stage of drying are mostly irrecoverable, as they are in the WRC (see, e.g., Fleureau et al. 1993; Peron et al. 2007). From now on, these two distinct domains of drying will be referred to as domain 1 ( $S_r$  equal to one, large and mostly irrecoverable strains; in Fig. 1, region of the plots to the left of air-entry value) and domain 2 (decreasing  $S_r$  with small strains; in Fig. 1, region of the plots to the right of air-entry value).

The drying free shrinkage scenario could be conceptualised as follows: (i) vapour pressure in the sample surroundings decreases, causing evaporation of the liquid water at the boundary of the material, and then (ii) a gradient of pore-water pressure (negative) is generated between the surface and the core of the sample, which induces an outgoing liquid-water flow (Coussy et al. 1998; Kowalski 2003). Because the water pressure decreases, the effective stress increases, and the matrix suffers an increasing internal compression. Therefore, the sample shrinks. Shrinkage during the drying of domain 1 should be seen as an elastoplastic consolidation via an effective stress increase. Several experimental studies (Fleureau et al. 1993; Peron et al. 2007) show that plastic compressibility (determined through

isotropic consolidation testing) is very close to the  $e$ - $\ln(s)$  slope of the drying of domain 1.

### Constrained desiccation tests

#### General observations on the crack pattern

Constrained desiccation tests were all performed on a support that created an axial restraint. After about 17 h drying time on this support (see schematic in Fig. 5), a series of six to eight cracks (most commonly seven) appeared, always in the direction parallel to the notches. Photographs of typical final crack patterns are shown in Fig. 14 (tests CDI3, CDI4, and CDI6).

The number of samples sorted as a function of the number of cracks is shown in Fig. 15. Considering the average value of seven cracks, the mean crack spacing on a given sample and at the moment when cracking ended was 4.1 cm. The repartition of crack spacings (for the samples exhibiting seven cracks) is shown in Fig. 16; 75% of the cracks were between 2 and 6 cm apart, 55% were between 3 and 5 cm apart.

In Fig. 17, an example of cracking pattern formation (three steps of tests CDI5) is shown. In all of the tests, no more than 2 h elapsed between the first and last crack appearances. Before parallel cracks appeared, slight cracking occurred at the two bottom corners in relation to the uplift of the extremities of the bar (see Fig. 18). The first fully developed crack appeared anywhere throughout the bar (as in Fig. 17 at a drying time of 16 h 30 min). Sometimes two cracks appeared simultaneously at a small distance apart (less than 1 cm), while the last few cracks had the tendency to appear in a narrow range of time (a few minutes; see Fig. 17, 18 h 2 min drying time, three cracks are simultaneously forming). Based on our tests results, we cannot definitively claim where the cracks start, either at the top or at the bottom of the slab.

Once the pattern of parallel cracks was formed, diffused cracking occurred in the soil between the notches and the rest of the soil mass. Each soil cell between two neighbouring cracks exhibited a slight upward curling. As soon as cracking started, caliper measurements were no longer representative of strains and hence, were abandoned.

#### Water content evolution

Constrained desiccation tests CD1b and CD2 consisted of measuring average water content and strains evolution of Bi-oley silt using exactly the same method as for the free desiccation tests. Fig. 19 shows the average gravimetric water content variation with respect to time obtained for tests CD1b and CD2 (referred to as “constrained desiccation” in Fig. 19). The evolution obtained for free desiccation is also re-plotted in Fig. 19. Up to cracking onset, the evaporative flux is not appreciably different from the one measured in the free desiccation tests. From the first crack appearance, the rate of drying increased appreciably and the final dried state was reached more rapidly than in the free desiccation tests. Cracking is expected to greatly increase the rate of drying, as it creates new evaporation surfaces.

#### Gravimetric water content – strain relationships before cracking

Strain evolution (mean strain values obtained from tests

CD1b and CD2) with respect to average water content below the liquid-limit value and before cracking is plotted in Fig. 20. The parallel notches noticeably decreased the value of measured axial strains compared with the unconstrained case. As already stressed, the caliper measurements give a unique value of strain in each direction and also reflect the average behaviour of the overall bar. As the support was not made of Teflon, some amount of friction also arose in the transverse direction. Indeed, strains in the transverse direction were lower than those in the analogous free desiccation tests for the same water content value. In turn, vertical strains were larger than those observed in free desiccation tests for the same water content. The values of strains at the onset of cracking for constrained tests CD1b and CD2 are compiled in Table 4, and are compared with the values obtained at approximately the same water content (24%) for free desiccation tests F5 to F9 (which were plotted in Fig. 11).

#### Crack openings

The detailed results of tests CDI1 to CDI6 are now addressed. Photos of the crack pattern formation were recorded. Fig. 21 is an extract of a film sequence (test CDI6, image analysis software used (Micromak 1998)). Cracks often started from one of the bar edges and reached the other edge in approximately 8–10 min. It appeared that cracks were fully developed about 20 min after crack onset. Crack opening evolved slowly after this time, in relation to drying shrinkage and bending of the newly formed cells. The cells containing the soil between the cracks acted as separate intact and independent bars, experiencing a characteristic curling at their extremities. The edges of the fully developed cracks were fairly parallel and could be characterized by a single average value of the opening. Openings of all the cracks for tests CDI1 to CDI6, measured once each crack was fully developed (at the moment identified using the image analysis software), are compiled in Table 5.

As the phenomenon is subjected to certain variability from one test to another, the mean value and standard deviation are given in Fig. 22. Nevertheless, a marked tendency for successive crack openings to decrease along the process is observed.

#### Discussion on the origin of stresses inducing cracking

Based on the CD and CDI test results, the origins of the pattern of stresses that lead to cracking are discussed. In reaction to any restraint in its shrinkage deformation, a total stress increment,  $d\sigma_{ij}$ , arises in the considered element of soil. Such a stress increment could be expressed by

$$[3] \quad d\sigma_{ij} = D_{ijkl}d\varepsilon_{kl}^m = D_{ijkl}(d\varepsilon_{kl} - d\varepsilon_{kl}^h)$$

where  $D_{ijkl}$  is a tangent stiffness matrix,  $d\varepsilon_{kl}^m$  refers to the mechanical strain increment responsible for stress generation,  $d\varepsilon_{kl}$  is the observed strain increment, and  $d\varepsilon_{kl}^h$  is the shrinkage strain increment occurring if desiccation is not constrained (further referred to as “free” desiccation strain increment). The drying process may induce a significant increase in soil stiffness as well. Thus, in addition to constraint-induced strains, tensile stress generation in a soil undergoing desiccation also depends on changes in soil stiffness. Here, the focus is primarily on the role of

**Fig. 14.** Examples of final crack patterns.

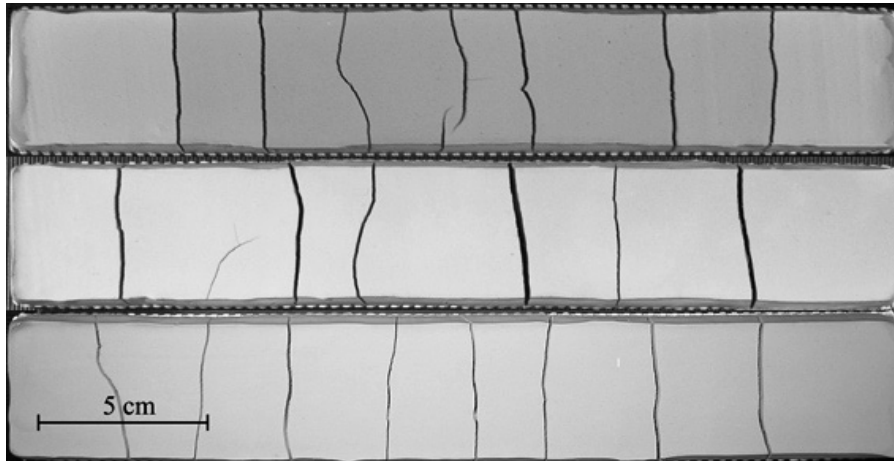


**Fig. 15.** Repartition of samples with respect to the number of cracks.

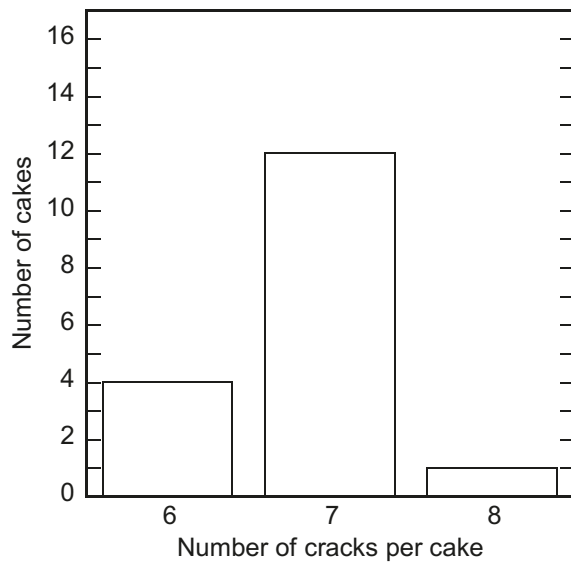


**Fig. 16.** Repartition of crack-spacing values.

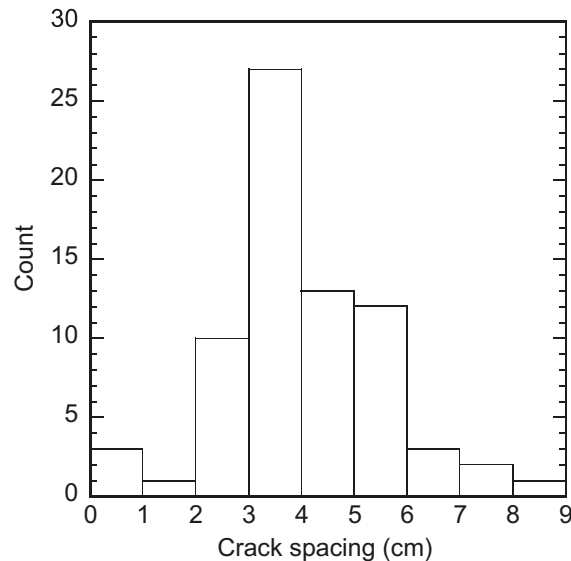


**Fig. 17.** Three steps of cracking pattern formation, test CD15.

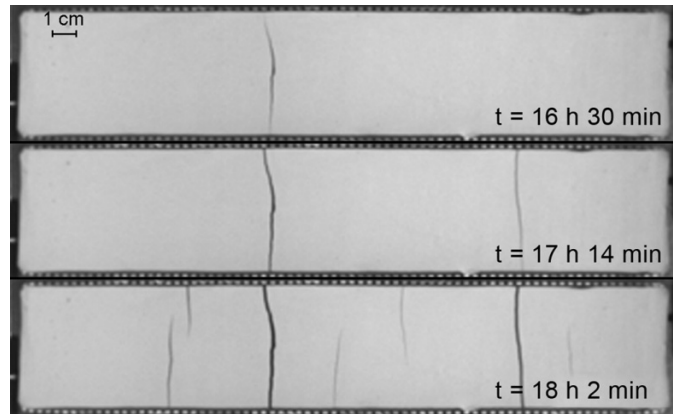
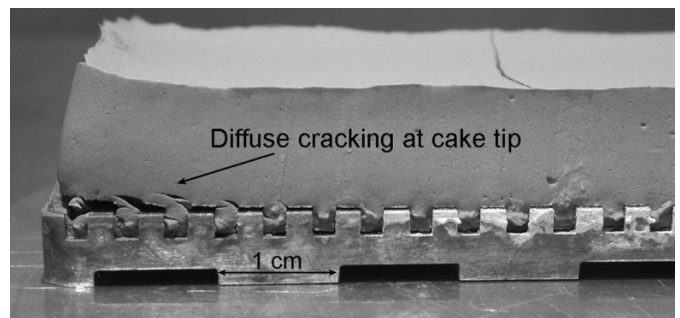


**Fig. 18.** Details of bar extremity showing slight cracking between the support and the rest of the bar.



constraint-induced strains. Note that this is a single-phase approach. No pore-water pressure and (or) effective stress effects are addressed. For an effective stress macroscopic approach to soil drying, see Nuth and Laloui (2008).

In the discussed experimental setup, the constraint-induced stress may arise due to (i) boundary constraints or (ii) strain proportional to water-content changes, which do not satisfy strain-compatibility conditions. Given that the successions of cracks are all observed to be parallel to the notches, it is concluded that the notch-induced constraints of type (i) in the axial direction are responsible for cracking. Reaction forces at the constraints induce tensile stress in the

**Fig. 19.** Gravimetric average water content evolution for constrained desiccation tests and comparison with the free tests.

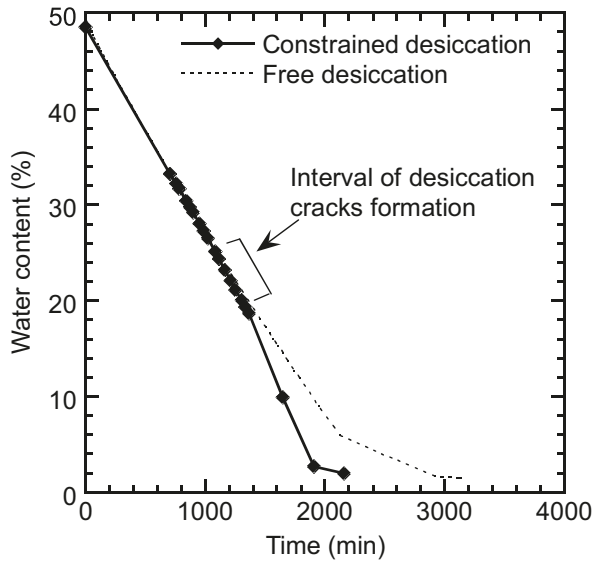


**Fig. 20.** Strains evolution versus average water content for constrained desiccation tests.

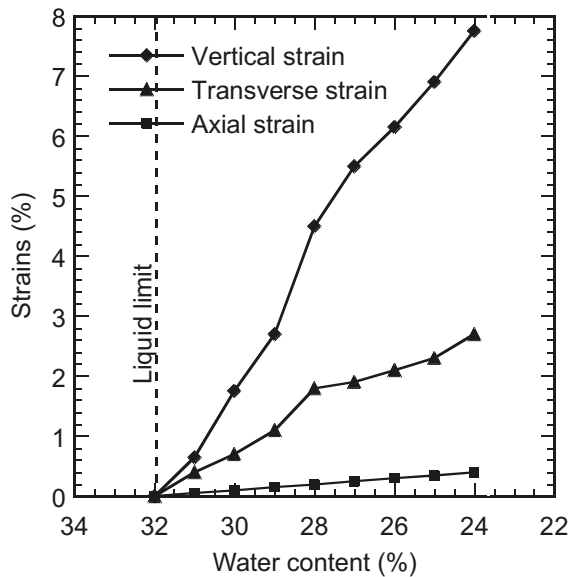
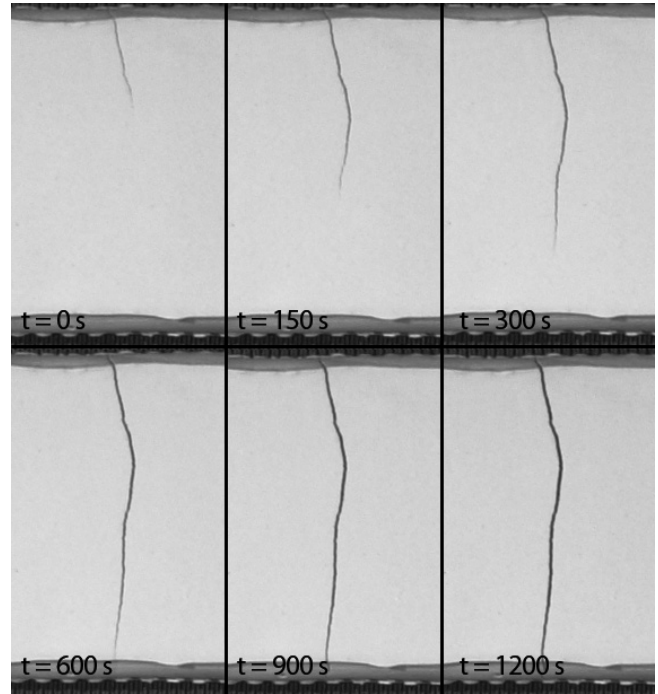


**Table 4.** Strain values for constrained desiccation tests and counterpart free test values at the same water content.

Desiccation tests	Strain component (mean values)		
	Axial (%)	Transverse (%)	Vertical (%)
Constrained	0.4	2.8	7.8
Free	4.0	3.9	4.6

axial direction, which may reach the tensile failure criterion. Lack of cracks in the other directions reflects the lack of (or minor) constraints in those directions. It is emphasised that only a slight water-content gradient has been measured along the axial direction (about 2% difference between the centre and the extremities), which is no longer observed be-

**Fig. 21.** Sequence of photos showing crack opening (CDI6 test).



low  $w = 25\%$ , and no noticeable vertical moisture gradient has been measured.

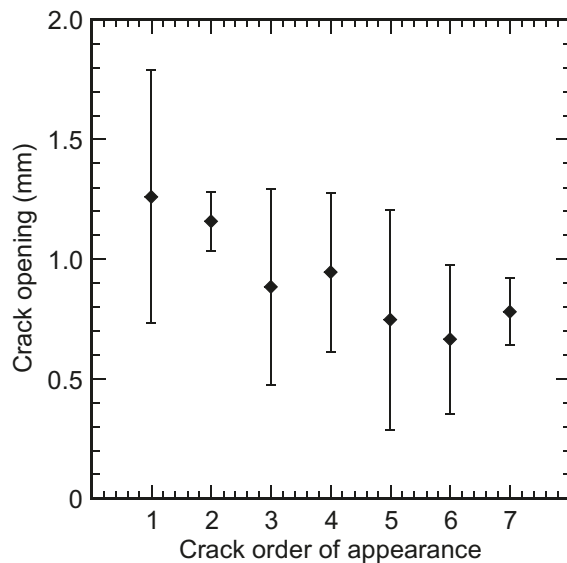
In Fig. 23, the mechanical strain components (equal to the difference between observed constrained desiccation strain and free desiccation strain) are plotted versus overall water content up to the first crack appearance, at  $w = 24\%$ . As the sample loses its water, it experiences a measurable mechanical strain (negative in tension): for the tested material, the strain threshold value, above which cracking occurs, can be estimated to be  $-3.5\%$  in the axial direction. All strains are average total strains assuming their uniformity along the sample. While the sample experiences traction in both horizontal directions, a vertical contraction is observed.

It needs to be pointed out that Fig. 23 reports, among other things, the average axial mechanical strain across the sample (as well, Fig. 20 reports the average axial strains). This may suggest that these strains are uniformly distributed across the sample. This is not exactly the case (see Fig. 9 for the situation of free tests). Notably, the displacement was measured at mid-height of the bar extremity. It is visible in Fig. 18 that the edge profile at the sample extremity is irregular. This is ignored and it is considered that the extremity edge remains vertical as the bar dries. In other words, it is considered that during constrained desiccation tests, the bar shrinks axially in an amount equal to the measured mid-plane axial strain. The idea is to treat the dried bar as an elementary representative volume subjected to a homogeneous state of stress and strain. While this is not exact in reality, it is a useful approximation for the present simple theoretical analysis.

Cracking is seen as resulting in a release of the stresses that were built up until a critical moment (i.e., when tensile strength is reached). If elastic one-dimensional behaviour is assumed, the crack opening produced by such a release must equal the total amount of mechanical axial strain built up

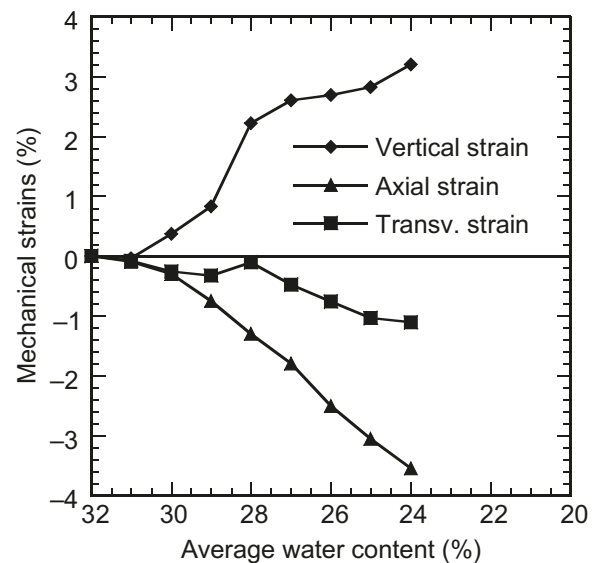
**Table 5.** Crack opening: measured values for all CDI tests.

Test No.	Crack opening (mm)						
	Crack 1	Crack 2	Crack 3	Crack 4	Crack 5	Crack 6	Crack 7
CDI1	1.90	1.30	1.00	0.60	0.10	0.90	0.90
CDI2	—	1.18	0.75	0.77	—	—	—
CDI3	0.78	1.19	0.76	0.78	0.78	0.86	0.70
CDI4	0.66	1.17	0.44	1.58	—	—	—
CDI5	1.58	1.18	1.19	1.25	1.11	—	—
CDI6	1.38	0.92	0.46	0.90	0.94	0.31	—
Mean	1.26	1.16	0.88	0.94	0.74	0.69	0.80
Standard deviation	0.53	0.13	0.41	0.33	0.46	0.33	0.14

**Fig. 22.** Crack opening with respect to the order of crack appearance (CDI tests).

before cracking. Transverse and vertical directions are considered to be unaffected by any constraint. This is a simplifying assumption, as the results revealed that there was a small constraint in the transverse direction. A rough calculation leads to a crack opening value between 10 mm (assuming the mechanical strain is  $-3.5\%$ ) and 18 mm (assuming the mechanical strain is  $-6\%$ , which is the largest value one can expect considering the experimental error). This value is significantly higher than the average measured value for the first crack opening (1.3 mm, see Fig. 22) and is also higher than the sum of all crack openings (6.5 mm).

It is likely that successive cracks should also first release a subsequent re-build-up of stresses due to subsequent partially constrained desiccation. This can be supported by the fact that successive cracks appear at somewhat lower total water content. More fundamentally, the discrepancy between the value of the crack opening calculated above on the one hand and the observed one on the other may be related to a dissipation process that occurs before cracking. This actually directly relates to the deformational behaviour within domain 1, in which strains are mostly irreversible.

**Fig. 23.** Difference between strains observed in free and constrained tests. Transv., transverse.

#### *Water content and suction of Bioley silt at the site and time of cracking*

The following discusses the results intended to determine suction, water content, and saturation conditions at cracking for Bioley silt dried in constrained conditions. The characteristics of the tests CSW, CSST, and CSSF are listed in Table 3; results of the measurements are given later in the section entitled "Analysis of experimental results".

#### *Water content measurements (tests CSW 4–6–12)*

The first crack appeared at an average water content of about 24% and the last crack at about  $w = 22\%$ , which is a notably narrow range. At this stage of drying, according to Fig. 8, the water content difference between the centre and the extremities of the bar has disappeared.

Details of the results are given in Table 6. All the measured average water contents, with a mean value calculated for each crack, are compiled in this table. Local water contents, measured in the vicinity of each newly formed crack, are also listed. Local water content values in the crack vicinities were always remarkably close to 22%–23% for all

**Table 6.** Summary of CSW test results (cracking local water content for Bioley silt).

Crack order of appearance	Test No.	Average values			Local values		
		Water content (%)	Mean (%)	Suction deduced from WRC (kPa)	Water content (%)	Mean (%)	Suction deduced from WRC (kPa)
<b>1</b>	CSW4	24.50	<b>24.1</b>	<b>89</b>	23.39	<b>22.6</b>	<b>115</b>
	CSW6	22.71			22.48		
	CSW12	25.69			21.85		
	PC1*	23.40			22.50		
<b>2</b>	CSW4	23.89	<b>23.4</b>	<b>85</b>	22.87	<b>22.9</b>	<b>90</b>
	CSW6	22.90			23.17		
	CSW12	—			22.64		
<b>3</b>	CSW4	22.95	<b>22.2</b>	<b>130</b>	23.68	<b>23.1</b>	<b>87</b>
	CSW6	21.53			22.55		
<b>4</b>	CSW4	22.95	<b>22.2</b>	<b>130</b>	23.21	<b>22.8</b>	<b>102</b>
	CSW6	21.53			22.32		
<b>5</b>	CSW4	22.95	<b>22.3</b>	<b>127</b>	22.99	<b>22.8</b>	<b>102</b>
	CSW6	21.70			22.57		
<b>6</b>	CSW4	22.23	<b>22.2</b>	<b>130</b>	22.52	<b>22.5</b>	<b>116</b>
	CSW6	22.24			22.53		
<b>7</b>	CSW4	22.50	<b>22.2</b>	<b>130</b>	22.57	<b>22.5</b>	<b>119</b>
	CSW12	21.98			22.46		
			<b>Mean</b>			<b>22.7</b>	<b>104</b>

\*Sample from another batch of tests, not addressed here.

**Fig. 24.** Sample average water content values with respect to crack order of appearance.

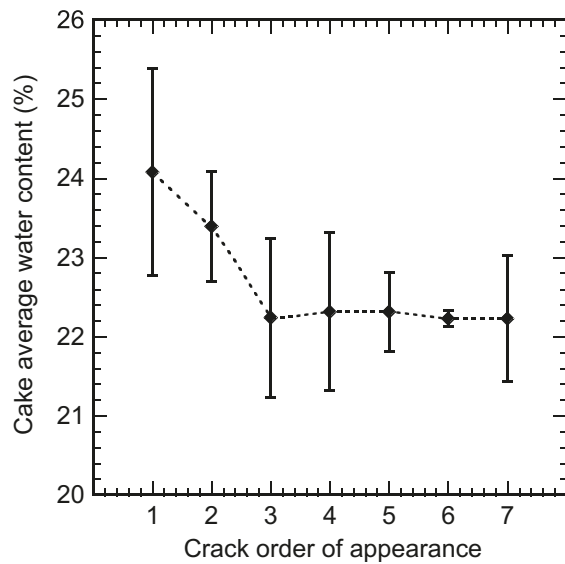
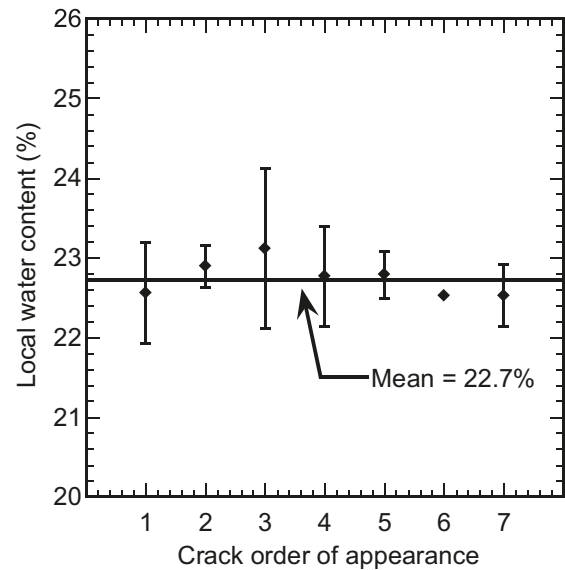


**Fig. 25.** Water content values in the vicinity of each crack with respect to crack order of appearance.



cracks, irrespective of their order of appearance (mean equal to 22.7%). As a relatively large number of measurements was performed (two to four water content measurements per crack), some statistics have been calculated to assess the variability of the measurements. The obtained average and local water content values are plotted in Figs. 24 and 25, respectively. In the plots, the vertical bars denote the standard deviation of each water content measurement. The average trend denoted in Fig. 24 (i.e., the early cracks appear at decreasing water content values and the last cracks tend to appear simultaneously at close water content values) could

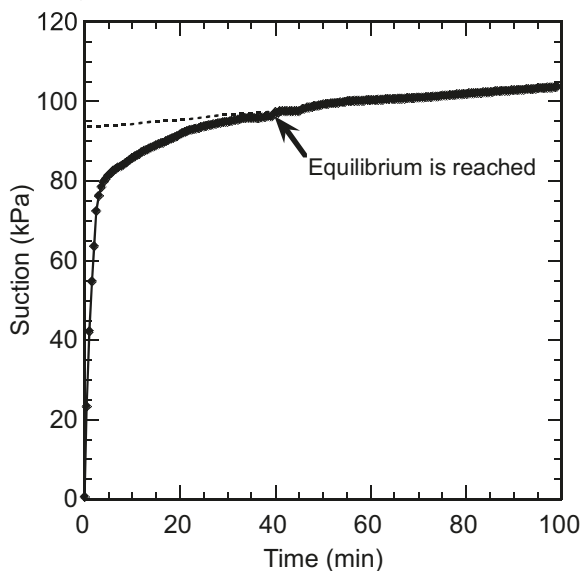
already be observed in Fig. 17 (photographs of three instances of cracking, test CDI5).

*Suction measurements at the crack (tests CSST 3–8–21 and CSSF 9 to 20)*

First, for each crack, an average and a local suction value have been deduced from the mean average water content and local water content values, respectively, using the WRC experimental water content–suction relationship (Peron et al. 2007). In the vicinity of each crack, suction values were always close to 80–120 kPa (overall mean value 104 kPa) for all cracks. Details of the values can be found in Table 6.

**Table 7.** Summary of suction measurement results for Bioley silt (tests CSS).

Test	Cracking local suction (kPa)	Cracking local water content (deduced from WRC) (%)
<b>Tensiometer</b>		
CSST3 (first crack)	90	
CSST8 (first crack)	94	
CSST21 (seventh crack)	92	
<b>Mean value</b>	<b>92</b>	<b>22.8</b>
<b>Filter paper</b>		
CSSF15 (seventh crack)	131	
CSSF16 (first crack)	58	
CSSF17 (first crack)	55	
CSSF20 (seventh crack)	60	
<b>Mean value</b>	<b>76</b>	<b>24.3</b>

**Fig. 26.** Suction measured by mini-tensiometer with respect to time (test CSST8).

Suctions at the crack were then measured with the mini-tensiometer (UMS GmbH 2001, see results in Table 7). A typical response of the mini-tensiometer is shown in Fig. 26 (test CSST8). Once the probe was inserted into the sample, suction reached a gentle linear evolution stage after 30 to 40 min. At this time, it was assumed that the pressure inside the probe reached equilibrium with the soil suction when a linear drift related to the ongoing drying process was attained, inducing a progressive suction increase. The value of suction at the very moment of insertion of the probe was deduced by subtracting this linear drift from the general response of the device.

For the test CSST3, after 2 h of measurements, a sudden suction decay was observed and within a few minutes, the measured suction had dropped to zero. This may be explained by the cavitation phenomenon. A cavitation mechanism within the tensiometer has already been suggested by Tarantino and Mongiovi (2001), due to the presence of small gas nuclei in the porous ceramic interstices. The ce-

ramic stone tip at this time was no longer in contact with the soil. The contact with air may have caused rapid desaturation of the ceramic stone, leading to air penetration inside the water reservoir. After this measurement, the probe was re-saturated (see section entitled “Water content and suction measurements at the time of cracking”).

Suction values measured with the tensiometer were between 90 and 94 kPa (see Table 7). In this range, the degree of saturation is still very close to 100% (WRC, Peron et al. 2007). On the basis of the three performed measurements, suction at cracking time appears to be irrespective of the crack order of appearance. The obtained mean value of suction (92 kPa) does not differ noticeably from the mean deduced from the water content measurements (104 kPa).

The filter-paper measurements (tests CSSF) are listed in Table 7 and offer much less consistent results. Results of tests CSSF9 to CSSF12 were eliminated. Filter-paper water contents were abnormally high. Consequently, the suction values deduced from the calibration curve were abnormally low compared with the expected values. For these tests, a light pressure was applied to the soil sample with the filter paper inside during the equilibration period. This may have affected the measurement quality. Matric suction values deduced from the calibration curve for the rest of the tests (CSSF15 to CSSF20) vary between 55 and 131 kPa (see Table 7). Although the scatter is very high, the mean value (76 kPa) is not far from the tensiometer value. The local water content values at the crack onset that are deduced from the soil WRC using the suction measurements with the tensiometer and filter papers are also given in Table 7.

#### *Influence of the initial water content on the suction and water content at the moment of cracking (tests CSI 5–7–13–19)*

Characteristics of the CSI tests are given in Table 3. Those tests were performed in the same conditions and with the same techniques as tests CSST, CSSF, and CSSW discussed above, but with varying initial water content. Results are compiled in Table 8. Suction or water content values deduced from the WRC are also reported. No measurable influence of the initial water content on the values of water content and suction at the moment of cracking can be identified.

#### *Saturation state in the vicinity of newly formed cracks*

The degree of saturation at cracking was deduced from the  $S_r$ - $s$  relationship of the WRC. The suction value at the moment of cracking was either determined from water content (by oven drying) on the basis of the  $s$ - $w$  relationship or by direct measurement (tensiometer or filter paper), both values being very close (see also Table 7). As already stated, the WRC was determined by a volume-displacement method that greatly minimizes the experimental error on the volume measurement. The experimental error on the degree of saturation was systematically estimated and turned out to be less than 2.5% (Peron et al. 2007). This ensured a reliable value of the deduced degree of saturation values. From suction measurements, the local degree of saturation corresponding to WRC is about 96% (Fig. 27). Cracking therefore takes place near the air-entry suction, assuming that air-entry suction corresponds to a degree of saturation equal to 100% based on the extrapolated Van Genuchten graph (see section entitled “Water retention curve determination”).

**Table 8.** Cracking local suction and water content using different initial water content values for Bioley silt (CSI tests).

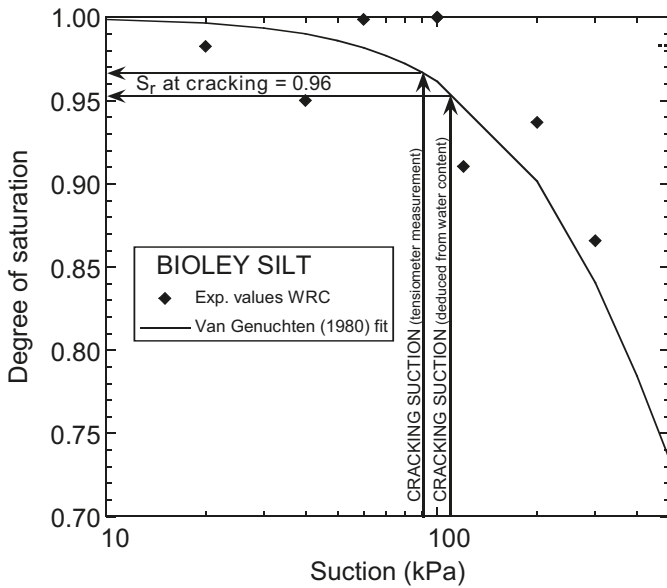
Test	Initial water content (%)	Crack No.	Local water content at cracking	Local suction at cracking (kPa)
CSW, CSS	48	—	22.7 <sup>a</sup>	90, <sup>b</sup> 104 <sup>c</sup>
CSI5	43.5	1, 2	22.5	115 <sup>c</sup>
CSI7	44.4	1	24.2	77 <sup>c</sup>
CSI13	41.4	1	23.1 <sup>c</sup>	84 <sup>b</sup>
CSI19	42.2	7	22.8 <sup>c</sup>	92 <sup>b</sup>

<sup>a</sup>Mean value.

<sup>b</sup>Tensiometer.

<sup>c</sup>Deduced from WRC.

**Fig. 27.** Degree of saturation at the time of cracking deduced from CSW and CSS tests. Exp., experimental.



**Comparison with other materials (tests CSX)**

Characteristics of the CSX tests (local cracking water content and suction measurements carried out on different materials) are given in Table 3. The results are compiled in Table 9. With La Frasse clay, a sufficiently large number of tests have been performed to make the same conclusion as for Bioley silt, i.e., local water content and suction at the time of cracking are nearly constant, irrespective of the crack order appearance. The degree of saturation at the time of cracking can also be deduced from the corresponding local water content and suctions, using the  $s$ - $S_r$  relationships of the respective WRC. Values between 0.95 and 0.99 for Sion silt, and approximately equal to 0.93 for La Frasse clay, are obtained (Figs. 28 and 29). The corresponding suction values are 35–54 kPa (Sion silt) and 355 kPa (La Frasse clay). The conclusion that can be drawn about the desiccation cracking of these materials is the same as for Bioley silt: at the time of cracking onset, the degree of saturation is only slightly below 100% and the soil suction is close to the air-entry value.

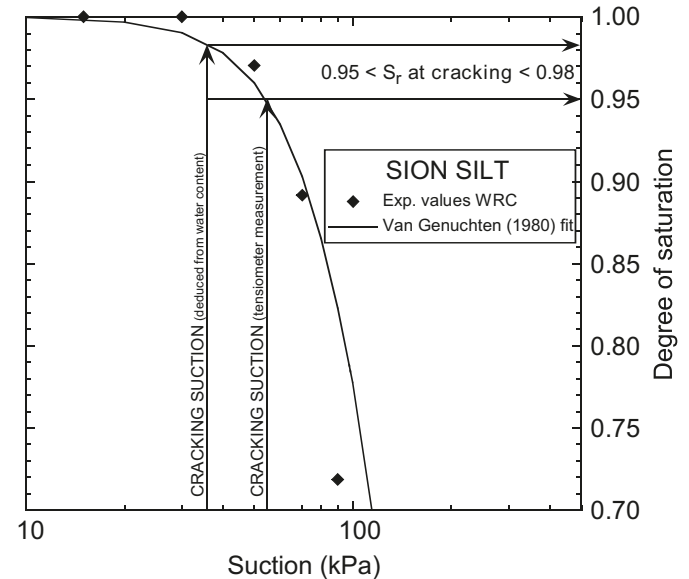
**Table 9.** Local cracking suction and water content values using different soils (CSX tests).

Test	Local water content at cracking (%)	Local suction at cracking (kPa)
<b>Sion silt</b>		
CSX23	25.11 (crack 1)	30 <sup>a</sup>
CSX24	26.12 (crack 1)	40 <sup>a</sup>
CSX25	23.3 (unknown crack No.) <sup>a</sup>	54 <sup>b</sup>
<b>Mean</b>	<b>24.8</b>	<b>54,<sup>b</sup> 35<sup>a</sup></b>
<b>La Frasse clay</b>		
CSX26	18.29 (crack 1)	400 <sup>a</sup>
CSX27	19.47 (crack 1)	350 <sup>a</sup>
CSX27	18.61 (crack 2)	410 <sup>a</sup>
CSX27	19.84 (crack 4)	330 <sup>a</sup>
CSX27	20.39 (crack 5)	290 <sup>a</sup>
CSX27	19.75 (crack 6)	340 <sup>a</sup>
CSX27	19.43 (crack 7)	360 <sup>a</sup>
<b>Mean</b>	<b>19.4</b>	<b>355 kPa<sup>a</sup></b>

<sup>a</sup>Deduced from WRC.

<sup>b</sup>Tensiometer.

**Fig. 28.** Degree of saturation at the time of cracking (Sion silt). Exp., experimental.



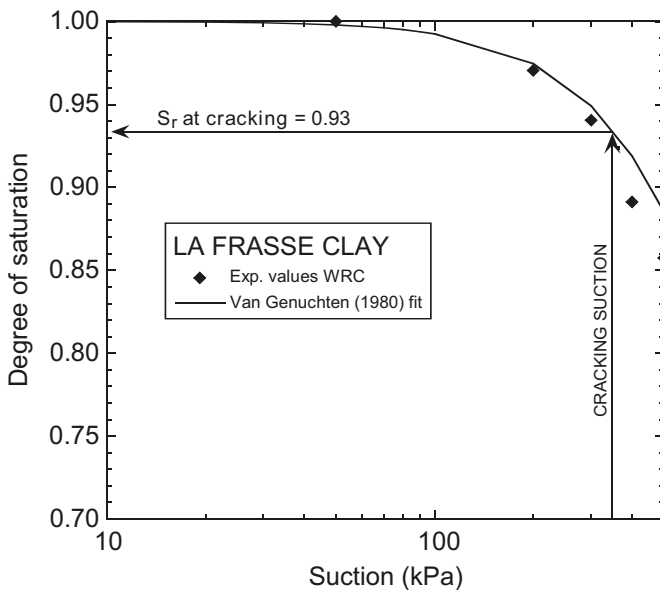
**Summary of test results: cracking water content and suction**

In the discussed test conditions, at the time of cracking, the water content and suction of Bioley silt prepared as an initially saturated slurry were  $w = 22.7\%$  and  $s = 90$ – $104$  kPa, respectively, depending on the measurement method (tensiometer or indirect measurement using the WRC). At that time, the local values of the degree of saturation near the crack were all between 93% and 99% and the soil suction was close to the air-entry value. The same behaviour was observed for Sion silt and La Frasse clay.

**Discussion of the crack-initiation conditions**

Crack-initiation conditions are now discussed, starting from the test results regarding water content, suction, and degree of saturation at cracking. Many prior results (Corte

**Fig. 29.** Degree of saturation at the time of cracking (La Frasse clay). Exp., experimental.



and Higashi 1960; Ayad et al. 1997; Avila 2004; Nahlawi 2004; Rodríguez et al. 2007) are close to the present findings that desiccation cracking of initially saturated and remoulded soils occurs in domain 1, when the overall degree of saturation is 100%.

In an attempt to shed light on the role of air entry in crack initiation in saturated conditions, it may be useful to address phenomena arising during drying at the pore scale. Some studies propose that defects and air-filled pores may act as crack initiators in soils (Frydman 1967; Snyder and Miller 1985; Morris et al. 1992).

It may be of interest that the drying of gels has also demonstrated that cracking has a tendency to occur as the material degree of saturation is still very close to 100% (within the measurement error range), and its water content is not far from the shrinkage limit (Dwivedi 1986; Anderson and Klein 1987; Simpkins et al. 1989) in laboratory tests. Gels can be considered as highly deformable porous media with a solid phase consisting of a polymer network. This observation allows some interpretations at the gel pore scale (1 to 5 nm pores), which may be related to the present case. Cracking near the air-entry value has been linked to the formation of a drying front in the gel at the moment of air entry (Scherer 1990). The advancing drying front separates a zone where the gel is almost completely desaturated from a zone where the gel is still completely saturated. Such a front may be irregular due to the irregular pore fabric, particularly the existence of constricted pores, leading to a drying scenario such as that of Fig. 30. In the figure, the shaded area is water-filled pores and the white area represents air-filled pores. Drained zones with a certain extension, shape, and orientation with respect to the stress field could be considered as defects, increasing the probability of crack inception.

Water cavitation may be also a way for dry zones to appear directly inside water-filled pores. Cavitation is observable when the water pressure at a point falls below the water vapour pressure at the local ambient temperature. Water undergoes a phase change, creating vapour-filled voids,

termed cavitation bubbles. This situation is likely to occur for a suction value greater than about 100 kPa (atmospheric pressure), because the saturation vapour pressure of water at ambient temperature is very low (approximately 3 kPa).

The growth of a gas bubble requires overcoming an energy barrier. Or and Tuller (2002) recall that the energy required to form a gas bubble,  $\Delta E_B$ , is the sum of the energy of a newly created interface and the work of the negative pressure over the bubble volume, given by

$$[4] \quad \Delta E_B = 4\pi r_c^2 T_s + \frac{4\pi}{3} r_c^3 (p_a - p_w)$$

where  $r_c$  is the radius of the bubble,  $T_s$  is the water-vapour surface tension, and  $p_a - p_w$  is the difference between air and water pressure, which is often identified as the matric suction.

The maximum of this energy variation is reached for a bubble radius,  $r_c^*$ , equal to

$$[5] \quad r_c^* = \frac{-2T_s}{p_a - p_w}$$

which is the well-known Young–Laplace equation.

In other words, for a given (negative) pressure, bubbles smaller than the critical radius given by eq. [5] do not grow, as the energy required is larger than the maximum value. Above the critical radius, the energy of the system decreases with increasing bubble radius. Thus, cavitation is likely to occur for water pressures below its saturation vapour pressure and only from the bubbles with the critical radius (at a given pressure). Consequently, the smaller the critical bubble, the higher the suction that can be sustained without cavitation. A pressure deficit below atmospheric pressure, larger than 100 kPa, can be sustained.

There are two common cavitation circumstances to be distinguished. In case 1, there are no initial gas bubbles that could be acting as cavitation nuclei; hence, water can reach a very high suction value without experiencing cavitation. As tension increases, however, formation of a gas bubble, being energetically favourable, becomes more and more probable. This process is called homogeneous nucleation. In case 2, gas bubbles pre-exist in water (commonly the case). In this situation, cavitation occurs as soon as the water pressure reaches a value corresponding to the critical radius given by eq. [5].

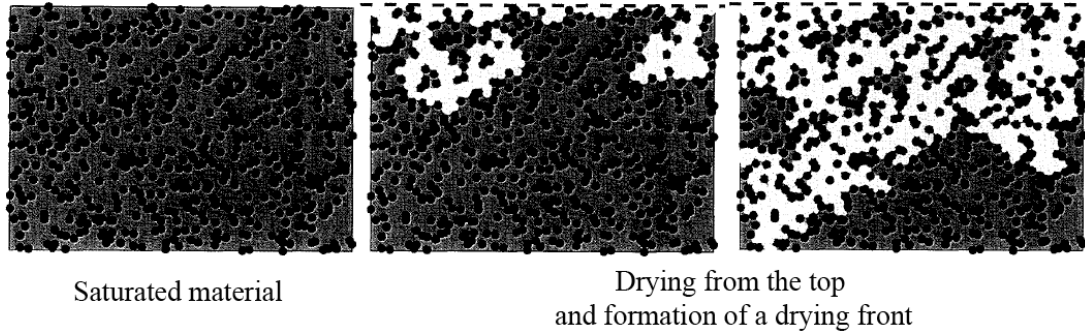
In case 1, the number of possible nucleations per unit time per unit volume of liquid,  $I_V$ , has been shown by Fisher (1948), using Maxwell–Boltzmann’s statistics, to be

$$[6] \quad I_V = \frac{N_A k_B T}{2\pi V_M \hbar} \times \exp \left\langle - \left\{ Q + \frac{16\pi T_s^3}{3[(p_a - p_w) + p_v]^2} \right\} / k_B T \right\rangle$$

where  $N_A$  is Avogadro’s number,  $k_B$  is Boltzmann’s constant,  $T$  is ambient temperature,  $V_M$  is the molar volume of water,  $\hbar$  is Dirac’s constant,  $Q$  is the activation energy for molecular transfer across the water–vapour interface, and  $p_v$  is the saturation vapour pressure.

The water (negative) pressure required to make a nuclea-

**Fig. 30.** Schematic cross section of a drying gel with constricted pores (after Scherer and Smith 1995, with permission from Elsevier).



tion rate of  $2.778 \times 10^{-6}$  possible at ambient temperature (meaning that one nucleation occurs in a volume of  $100 \text{ cm}^3$  of water, in a period of 1 h) is obtained using eq. [6] at a value of 123 MPa, corresponding to a bubble radius of about 1 nm (see eq. [5]). This calculation indicates that the range of suction (0–500 kPa) for which the material is likely to crack is largely below values that could involve observable homogeneous cavitation.

Thus, cavitation in the discussed materials would most probably be the consequence of heterogeneous nucleation. Again, a calculation using eq. [5] indicates that nuclei of about  $1.45 \text{ }\mu\text{m}$  are sufficient to initiate cavitation within the water mass at a negative pressure of about 100 kPa.

From the cracking onset point of view, in order for a formed bubble to grow out of the pore where it was created, suction in the surrounding water must be great enough to allow the water-vapour bubble to pass through the porous network. This condition was discussed by Scherer and Smith (1995) for drying gels and by Or and Tuller (2002) for soils. Thus, suction must be higher than the air-entry value. If this is the case, larger unsaturated pockets may be created, acting as flaws and possibly promoting crack initiation in the same way as discussed above. Such “pockets” may also appear earlier than the measured air entry in a given sample, depending on the existence of localized, larger pores that could be drained early in the process.

The direct application of the Young–Laplace law to the cavitation phenomenon has been found in many technical circumstances to be misdirected, and has led to incoherent results many times before (see e.g., Brennen 1995). This is especially valid in the case of homogeneous nucleation, where the initial size of cavities is linked to thermally activated water molecules themselves. Particularly for soil pore water, heterogeneous cavitation is thought to occur at the solid walls of pores, with the cavity radius determined by the pore geometry.

Based on the actual porosimetry data for Bioley silt and Sion silt (Peron 2008), a microscale hydromechanical model has been proposed to simulate the shrinkage deformation and subsequent cavitation occurring in different classes of pores (see Hu et al. 2008, 2009). The model exploits an earlier idea of Or and Tuller (2002), in which the size of a cavitation-created bubble is equal to the size of the soil pore. For a two-modal pore model, it was found that water in larger pores cavitates much earlier than in smaller pores. An averaged suction–saturation–deformation pattern seen in

macroscopic experiments has been reproduced by simulating a two-pore system (Hu et al. 2009).

In conclusion, the air-entry value (or better said the gas-entry value) can be associated with the formation of localized drained zones, either by cavitation near the existing interphase boundary by generating water vapour, which subsequently merges with the external gas environment, or by cavitation deep within the body followed by a migration or growth of the air bubbles, which subsequently act as material defects. These defects can then become crack inceptors. The latter scenario is related to the observation that locally, the moment of gas entry is critical for crack initiation in the discussed test conditions. However, the present tests do not give direct evidence of the effectiveness of such a mechanism.

The presence of defects must be invoked; a crack starts from some kind of inceptor. Macroscopically, tensile strength could be viewed as a property related to such defects (Peron et al. 2009a); similarly, suction and degree of saturation changes are also defect-related properties.

In the above consideration, the issue of scale of observation needs to be carefully addressed.

#### **General conclusions for constrained desiccation tests**

Stress generation during desiccation can be seen as a consequence of a kinematic constraint in suction-induced shrinkage deformation. The reaction that arises in response to such a constraint is at the origin of cracking.

It is emphasised that cracking occurs during an elastoplastic process, and any model dedicated to predicting its initiation should consider this. Cracking and the mechanical processes that precede it occur in domain 1 of desiccation (degree of saturation close to 100%). During this stage, in test conditions, a large portion of the deformation is irreversible. In the present case, it is during this stage that the tensile stress builds up to a critical point where the tensile strength is reached.

At a more refined scale, cracking onset, the air-entry value, and the shrinkage limit appear to be very close to each other, at least under the present constrained desiccation test conditions. It is noted here that this observation is confirmed by the evolution of the pore-size distribution during desiccation (Peron 2008); a microscale model by the authors addresses mechanisms associated with the role of constraints at a pore scale in attaining tensile strength.<sup>3</sup> Some observations on drying gels (Scherer 1990) show that, at the mo-

ment of air entry, localized drained zones form while the surroundings remain saturated; such heterogeneities may create defects and crack inceptors.

There are good reasons to presume that a relationship exists between the tensile strength and suction. The correspondence between the end of saturation (domain 1) and desiccation crack initiation more precisely suggests that there can be a dependence of the tensile strength on the degree of saturation and the suction air-entry value. Actually, suction evolution in the drying body alters the “interparticle force” (Mitchell and Soga 2005) on one hand, but also changes the liquid phase repartition and occupation of the porous space, possibly also altering the conditions for crack initiation during desiccation, on the other.

In addition, the dependence between the elasticity moduli and variables of suction and (or) saturation may also play a role in the addressed processes. However, this is hardly quantifiable using the present test results.

### Crack pattern tests

#### Test results

Six desiccation tests were performed (crack pattern tests CP0 to CP5, see section entitled “Crack pattern test procedure”), for which a bottom substrate was devised with two-dimensional constraints instead of the one-dimensional constraint considered so far. Slabs with two different heights (three slabs 4 mm high and three slabs 12 mm high) were tested.

All tested samples cracked, leading to formation of a bi-dimensional net of cracks (see Figs. 31 to 34). Marked differences were observed between samples that were 4 mm high and samples that were 12 mm high. The former ones experienced a large number (from 160 to 352, see Fig. 31) of relatively thin cracks; the latter ones experienced a small number of relatively wide cracks (from 16 to 31 depending on the tests, see Fig. 32). Corte and Higashi (1960) observed the same trend when drying similar square-shaped slabs.

Crack intersecting angles were also measured. Generally, cracks intersect at about  $90^\circ$ , up to about  $150^\circ$ . Angles above and beyond this range are rare. During tests CP0 and CP3 (4 mm high), it was observed that some groups of three cracks intersecting at  $120^\circ$  had the tendency to appear simultaneously, especially at the beginning of the cracking stage (Fig. 33, circled cracks). Upon further desiccation, the crack pattern changed and cracks tended to meet other existing cracks that formed an angle of about  $90^\circ$  (Fig. 34, photograph taken 4 h later than Fig. 33, when all the cracks were formed). The number of cracks and mean intersection angle for each test are listed in Table 10. It appears that a two-dimensional constraint tends to originate two limiting types of crack patterns:  $90^\circ$  intersecting and  $120^\circ$  intersecting cracks. It can be deduced from the present test results (tests CP and previous constrained desiccation tests CD) that the geometry of the crack pattern depends strongly on the nature of the boundary constraint and the sample geometry. In addition, as moisture gradients are likely to induce tensile stress generation, the resulting crack pattern is also likely to depend on the boundary flux conditions.

Fig. 31. CP2 test, final stage of cracking.

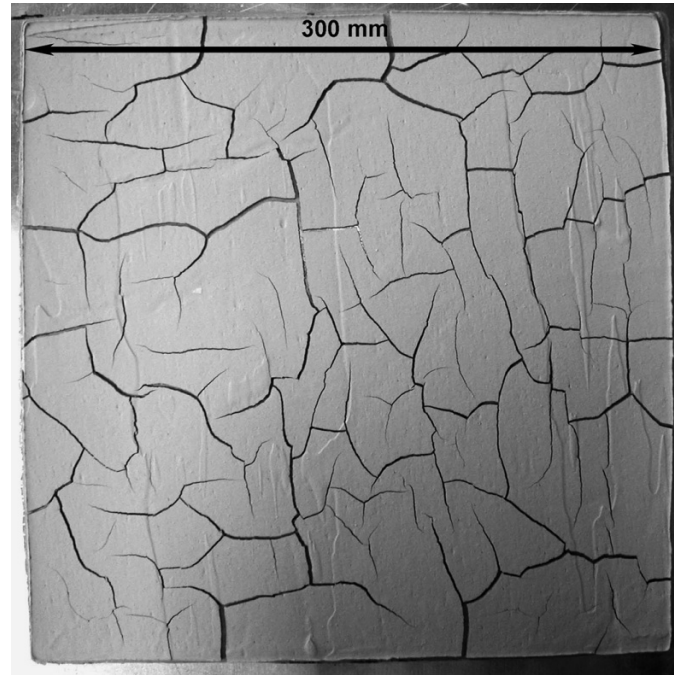
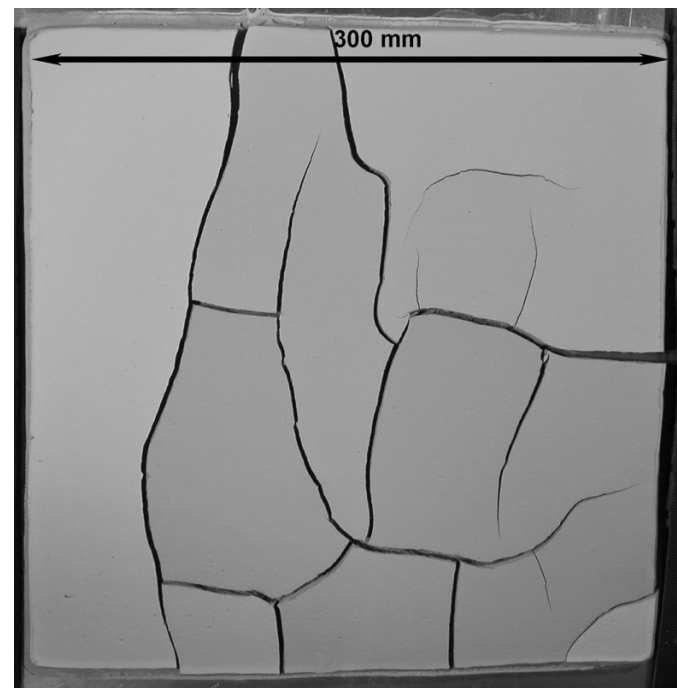


Fig. 32. CP5 test, final stage of cracking.



#### Interpretation of crack pattern geometries

The main characteristics of the observed crack patterns, i.e., their orientation and spacing, are now addressed by making use of basic energy concepts. An issue of the optimization of the drying velocity of a solid was recently addressed by Bejan (2000) via an energy approach.

Both patterns obtained in the present crack pattern tests (CP0 to CP5) and in constrained desiccation tests presented earlier are addressed. Here, propagation and formation of a given pattern of cracks, once initiated, is approached from

**Fig. 33.** CP0 test, initial stage of cracking: 120° intercepting cracks circled.

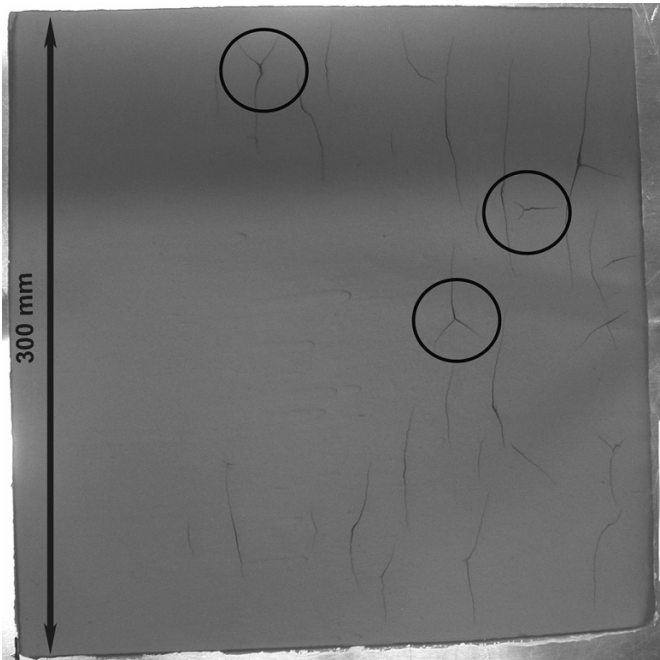
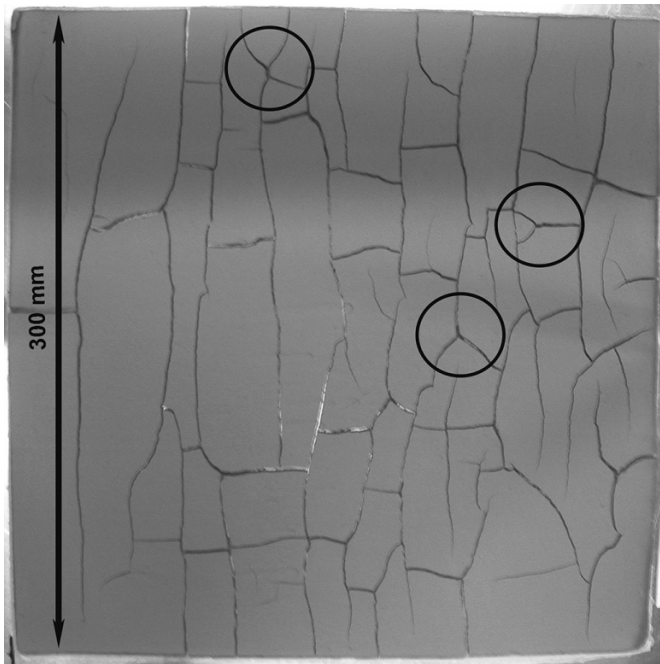


**Fig. 34.** CP0 test, final stage of cracking: 120° intercepting cracks circled.



the point of view of fracture mechanics. The overall energy balance at the time of cracking can then be considered.

The interpretation of cracks intersecting at 90°, widely observed in our CP tests, is straightforward. Once a crack has formed, tensile stresses perpendicular to the crack axis are released near the crack. A propagating crack, when approaching the vicinity of another existing crack, tends to orient in the direction perpendicular to the local maximum tensile stress, i.e., parallel to the existing crack.

**Table 10.** Intercepting angle and number of cracks of CP tests.

Test	Sample height (mm)	Number of intercepting cracks	Mean interception angle (°)
CP0	4	194	99
CP1	12	20	91
CP2	4	160	110
CP3	4	352	101
CP4	12	31	101
CP5	12	16	95

The case of 120° intersection angles, less frequent in the CP tests configuration, results from an energy minimization process, as demonstrated for soils earlier and reported by Corte and Higashi (1960). Cracking, by creating new solid surfaces, is an energy-consuming process. Consider an infinite slab subjected to a horizontal two-dimensional constraint while it dries. If the tensile stress at a given point is the same in any horizontal direction, then the sample tends to crack along several planes of failure. Of the infinite theoretical possibilities, failure will occur in three planes oriented at 120°, because this geometry produces the lowest crack area enclosing the maximum soil volume and thus, enables the consumption of a minimum surface energy per unit volume. This reflects the tendency of any physical process to do the most with the least.

**Estimation of crack spacing based on the cracking process energy**

In the following, a formula determining the spacing of parallel cracks is developed. The constrained desiccation test patterns are addressed. It is assumed that

- (1) The soil sample has a length  $L$ , width  $l$ , and height  $h$ .
- (2) Immediately prior to cracking, the soil sample is subjected to an axial tensile stress (the minor principal stress) equal to the tensile strength, and cracks are caused by constrained desiccation in this direction because shrinkage is totally free in the other directions.
- (3) Immediately after cracking, the soil contains a system of  $N_c$  cracks with a spacing  $d_c$ .
- (4) The cracks have propagated from their initial depth  $a_{c0}$  to their final depth  $a_{cf}$ .

Energy conservation requires the elastic strain energy,  $U$ , released due to crack formation to be fully converted into the surface energy,  $W_s$ , of newly formed cracks. This principle is then applied.

The number of cracks  $N_c$  is linked to the spacing by

$$[7] \quad N_c = \frac{L}{d_c} - 1$$

The energy  $W_s$  required to form the system of  $N_c$  cracks of initial depth  $a_{c0}$  and final depth  $a_{cf}$  is given by

$$[8] \quad W_s = N(a_{cf} - a_{c0})lG_c$$

where  $G_c$  is the energy release rate associated with crack growth. It is further considered that  $a_{cf}$  is equal to the sample height  $h$  (fully penetrating crack).

It is assumed that all the elastic strain energy  $U$  is released during the process of cracking. This is equivalent to

saying that both vertical and lateral stress components are zero. The axial stress vanishes when the bar cracks (the residual stress at the bottom of each newly formed cell between two cracks is neglected). In these conditions, and considering fully penetrating crack of depth  $h$  and the elastic energy of the whole volume of the bar, one arrives at

$$[9] \quad U = \frac{ELhl(\varepsilon_x^{m,e})^2}{2}$$

where  $E$  is Young's modulus and  $\varepsilon_x^{m,e}$  is the elastic part of the mechanical strain in the axial direction at the instant of cracking onset.

For the sake of simplicity, it is considered that strain is prevented in the axial direction, which is not far from reality. The mechanical strain is thus equal in absolute value to the free strain. It is emphasised that only the elastic part of the strain should be included when calculating the stored energy (eq. [9]), considering that a large part of the deformations is irrecoverable.

Denoting  $\varepsilon_x^h$  as the "free" shrinkage strain, setting  $W_s$  and  $U$  equal, and neglecting the initial length  $a_i$  compared with the final length  $h$ , one arrives at the number of parallel cracks as

$$[10] \quad N_C = \left(\frac{E}{G_c}\right) \frac{L(\varepsilon_x^h)^2}{2}$$

Spacing  $d_c$  can be directly deduced from eq. [7]. This calculation conforms to the intuitive expectation that states that the more drying soil volume there is, the more cracks are likely to be formed. Comparable calculations (in the case of a moisture gradient forming from the drying surface) can be found in Bazant and Cedolin (1991) and in a more sophisticated way in Hong et al. (1997), without the simplifying assumptions of fully penetrating cracks and total strain energy release. In Bazant and Cedolin (1991), partial strain energy release is introduced via an empirical coefficient scaling the value of energy  $U$ .

To estimate the value of  $N_C$  for the Bioley silt constrained desiccation tests, the value  $G_c = 0.35$  N/m is chosen (taken from Ayad et al. (1997) for marine sensitive clay). The estimate of the elastic part of strain is reached considering  $E = 32 \times 10^6$  Pa (taken from the modulus determined in triaxial compression tests, Peron 2008). The strain  $\varepsilon_x^h$  is determined from the WRC results. If one assumes that during the loss of water content in the range from the liquid limit to cracking, suction increases from 5 to 100 kPa and the elastic part of shrinkage deformation (the free shrinkage strain,  $\varepsilon_x^h$ ) is 0.12%. With the above assumptions, a value of  $N_C = 19$  is obtained. This result is dependent on the choice of the energy-release rate  $G_c$ , which is not known for the present soil. For instance, Avila et al. (2002) report values of  $G_c$  varying from 3.8 to 6.5 N/m for lacustrine clay; the obtained crack number is then much smaller (with  $G_c = 6.5$  N/m,  $N_C = 1$ ). Incidentally, the estimated values ( $N_C$  ranging from 1 to 19) are not inconsistent with the observed crack spacing obtained in the constrained desiccation tests (i.e.,  $N_c = 7$ ).

This method of calculating crack number or spacing can be extended to the bi-dimensional case featuring  $120^\circ$  intersecting cracks that form hexagons. If the desiccation process

continues beyond the first crack, higher-order cracks can form in the cells of the soil isolated by previous cracks, following the same rules as stated above.

One can finally note that in the above analysis, the decomposition of total strain into a mechanical strain and a free shrinkage strain has been implicitly used; the mechanical behaviour is controlled by the total stress.

However, in the case of the CP test series, the proposed relation (eq. [10]) fails to explain the experimental evidence showing that crack spacing tends to increase with slab height. Considering a system of parallel cracks, Bazant and Cedolin (1991) propose a bifurcation analysis that could help in the understanding of the latter behaviour (the same interpretation was provided by Lachenbruch (1961) in a nonmathematical way). Bazant and Cedolin (1991) consider the case of a semi-infinite material volume subjected to drying from the surface. A dry zone thus propagates from this surface towards the interior of the volume. A fracture mechanics analysis leads to the conclusion that, while the first cracks are advancing from the surface, their effective spacing increases (discretely) as some of them stop and others proceed and eventually become critical. Therefore, if a semi-infinite slab is considered, the thicker the slab, the more cracks are bound to vanish and the larger the final crack spacing. This analysis holds only if a moisture gradient is developing in the material. This would also mean that in the CP tests, nonhomogeneous drying (from the surface) plays an important role in the crack pattern formation.

In the above analyses, the crack pattern could develop in the presence of a homogeneous stress field. Another approach for crack spacing derivation is possible in some cases, if the location of crack initiation naturally arises from the form of the stress field. The stress state then meets the material strength criterion, which includes the tensile strength component at some points, due to a particular body shape or boundary conditions.

In the situation of constrained desiccation tests, one can further consider that each crack fully penetrates the bar. The energy required for the crack propagation is then ignored and fracture mechanics and energy considerations are set aside. The crack spacing observed in constrained desiccation tests may well be explained in this way. The stress is likely to be the highest along the centre section of the bar (although the minor stress is almost constant in a large central part of the bar), so the first crack should split the bar in two equal pieces. As a first interpretation, successive cracks, as they appear at progressively lower total water content values, are the result of the constrained shrinkage in the newly formed bar segments. It is recalled that the entire formation of the observed crack pattern in the constrained desiccation tests lasted about 1.5 to 2 h, but a number of cracks appeared simultaneously.

With such reasoning, Groisman and Kaplan (1994) proposed to relate crack spacing to dried circular-slab height. If one considers a cell of soil between two adjacent propagating cracks, the (uniaxial) stress should theoretically be highest in the centre of the bottom-constrained cell. The total stress component in the horizontal direction,  $\sigma$ , is the ratio of the stretching force,  $T_c$ , acting on a unit length of the layer thickness,  $\sigma = T_c/h$ . Assuming that stretching is due to the bottom friction,  $T_c$  should be roughly proportional to the

linear dimension of the cell  $L$  in the direction of the force,  $T_c \approx L$ . Thus, the stress in this direction is  $\sigma = T_c/h \approx L/h$ . Therefore, the critical length,  $L_{cr}$ , of the cell, required to provide the stress  $\sigma_{th}$  under which the material breaks, is proportional to the thickness of the layer,  $L_{cr} \approx \sigma_{th}$ . The process of longitudinal fragmentation of the specimen must stop when the axial dimension of the cells drops below  $L_{cr}$ , as the bottom friction ceases to supply the stress needed for cracking. Similar considerations are found in Kodikara and Choi (2006).

In conclusion, if one assumes that cracks form successively through incremental growth to the material tensile strength in locations well defined by the stress field and the boundary conditions, it is relatively easy to interpret the formation of the crack pattern. Final crack spacing should be the consequence of changes in tensile strength or other material properties. When the crack pattern emerges from a homogeneous stress field, it is less straightforward as to how the observed process is quantified. Fracture mechanics should be invoked, i.e., global energy considerations. The discussed crack patterns may result from both types of processes, as experimentally cracks tend to appear either successively (at a clearly decreasing overall water content) or at the same time.

## Conclusions

The results of an experimental study of desiccation of initially saturated soil were presented. Three kinds of tests were considered: free desiccation tests, constrained desiccation tests, and crack pattern tests, all consisting in air drying under controlled conditions. The significance of these results was studied and some key variables quantified and discussed. The factors controlling shrinkage and cracking were examined. Based on this analysis, the following conclusions can be drawn:

- (1) Free desiccation tests on initially saturated slurries confirm the general characteristics well known from WRC studies, i.e., the existence of two distinct domains for drying shrinkage (domain 1 at a degree of saturation close to 100%, with mostly irreversible deformation, and domain 2 at a decreasing degree of saturation, with a much smaller deformation, mainly reversible).
- (2) The stresses that lead to cracking clearly result from the presence of restraining boundary conditions and (or) moisture gradients. Desiccation cracking occurs in domain 1 at nonzero suction and a degree of saturation close to 100%. During this stage, a large part of deformation is irreversible. Stress builds up to a critical point at which the tensile strength is met.
- (3) The experimental results presented in this paper show that cracking initiates close to the onset of desaturation. The increase of suction in the drying body alters the liquid phase repartition (degree of saturation) and occupation of the porous space; this possibly modifies the conditions for desiccation crack initiation during drying. Furthermore, this coincidence could be related to the fact that tensile strength evolves during drying. Indeed, it is known that the increase of suction induces an increase of the apparent cohesion.
- (4) Energy redistribution through the body following crack

initiation can explain the geometry of the resulting crack patterns (such as crack spacing and intersection).

## Acknowledgments

This work was funded by the Swiss National Science Foundation, grants 200020–109661 and 200021–101917, and the US National Science Foundation, grant No. 0324543. The authors would like to thank Anne Seibel for her contribution to the desiccation tests.

## References

- Abu-Hejleh, A.N.M. 1993. Desiccation theory for soft cohesive soils. Ph.D. thesis, University of Colorado, Boulder, Colo.
- Abu-Hejleh, A.N., and Znidarcic, D. 1995. Desiccation theory for soft cohesive soils. *Journal of Geotechnical Engineering*, **121**(6): 493–502. doi:10.1061/(ASCE)0733-9410(1995)121:6(493).
- Albrecht, B.A., and Benson, C.H. 2001. Effect of desiccation on compacted natural clay. *Journal of Geotechnical and Geoenvironmental Engineering*, **127**(1): 67–75. doi:10.1061/(ASCE)1090-0241(2001)127:1(67).
- Al-Khafaf, S., and Hanks, R.J. 1974. Evaluation of the filter paper method for estimating soil water potential. *Soil Science*, **117**(4): 194–199. doi:10.1097/00010694-197404000-00003.
- Anderson, P., and Klein, L.C. 1987. Shrinkage of lithium aluminosilicate gels during drying. *Journal of Non-Crystalline Solids*, **93**(2–3): 415–422. doi:10.1016/S0022-3093(87)80186-2.
- ASTM. 1994. Standard test method for measurement of soil potential (suction) using filter paper. ASTM standard D5298–94. ASTM International, West Conshohocken, Pa.
- ASTM. 2002. Standard test method for shrinkage factors of soils by the wax method. ASTM test method D4943–02. ASTM International, West Conshohocken, Pa.
- Avila, G.E. 2004. Estudio de la retraccion y el agritamiento de arcillas. Aplicacion a la arcilla de Bogota. Ph.D. thesis, Universitat Politecnica de Catalunya, Barcelona, Spain. [In Spanish.]
- Avila, G., Ledesma, A., and Lloret, A. 2002. Measurement of fracture mechanics parameters for the analysis of cracking in clayey soils. *In Unsaturated Soils: Proceedings of the 3rd International Conference on Unsaturated Soils (UNSAT 2002)*, Recife, Brazil, 10–13 March 2002. Edited by J.F.T. Jucà, T.M.P. de Campos, and F.A.M. Marinho. Swets & Zeitlinger, Lisse, the Netherlands. Vol. 2. pp. 547–552.
- Ayad, R., Konrad, J.M., and Soulié, M. 1997. Desiccation of a sensitive clay: application of the model CRACK. *Canadian Geotechnical Journal*, **34**(6): 943–951. doi:10.1139/cgj-34-6-943.
- Bazant, Z.P., and Cedolin, L. 1991. *Stability of structures: elastic, inelastic, fracture, and damage theories*. Oxford University Press, Oxford, UK.
- Bejan, A. 2000. *Shape and structure, from engineering to nature*. Cambridge University Press, Cambridge, UK.
- Brennen, C.E. 1995. *Cavitation and Bubble Dynamics*. Oxford University Press, Oxford, UK.
- Chertkov, V.Y. 2002. Modelling cracking stages of saturated soils as they dry and shrink. *European Journal of Soil Science*, **53**(1): 105–118. doi:10.1046/j.1365-2389.2002.00430.x.
- Corte, A., and Higashi, A. 1960. Experimental research on desiccation cracks in soil. U.S. Army Snow, Ice and Permafrost Research Establishment, Hanover, N.H. Research report 66.
- Coussy, O., Eymard, R., and Lassabatère, T. 1998. Constitutive modelling of unsaturated drying deformable porous media. *Journal of Engineering Mechanics*, **124**(6): 658–667. doi:10.1061/(ASCE)0733-9399(1998)124:6(658).

- Daniel, D.E., and Wu, Y.K. 1993. Compacted clay liners and covers for arid sites. *Journal of Geotechnical Engineering*, **119**(2): 223–237. doi:10.1061/(ASCE)0733-9410(1993)119:2(223).
- Dwivedi, K. 1986. Drying behavior of alumina gels. *Journal of Materials Science Letters*, **5**(4): 373–376. doi:10.1007/BF01672329.
- Fisher, J.C. 1948. The fracture of liquids. *Journal of Applied Physics*, **19**(11): 1062. doi:10.1063/1.1698012.
- Fleureau, J.M., Kheirbek-Saoud, S., Soemitro, R., and Taibi, S. 1993. Behavior of clayey soils on drying-wetting paths. *Canadian Geotechnical Journal*, **30**(2): 287–296. doi:10.1139/T93-024.
- Frydman, S. 1967. Triaxial and tensile strength tests on stabilized soil. *In Proceedings of the Third Asian Regional Conference on Soil Mechanics and Foundation Engineering*, Haifa, Israel, 25–28 September 1967. Jerusalem Academic, Jerusalem, Israel. pp. 269–275.
- Groisman, A., and Kaplan, E. 1994. An experimental study of cracking induced by desiccation. *Europhysics Letters*, **25**(6): 415–420. doi:10.1209/0295-5075/25/6/004.
- Guan, Y., and Fredlund, D.G. 1997. Use of the tensile strength of water for the direct measurement of high soil suction. *Canadian Geotechnical Journal*, **34**(4): 604–614. doi:10.1139/cgj-34-4-604.
- Holtz, R.D., and Kovacs, W.D. 1981. *An introduction to geotechnical engineering*. Prentice Hall, Upper Saddle River, N.J.
- Hong, A.P., Li, Y.N., and Bazant, Z.P. 1997. Theory of crack spacing in concrete pavement. *Journal of Engineering Mechanics*, **123**(3): 267–275. doi:10.1061/(ASCE)0733-9399(1997)123:3(267).
- Hu, L.B., Hueckel, T., Peron, H., and Laloui, L. 2008. Desiccation shrinkage of unconstrained soil in the saturated phase. *In Unsaturated Soils: Advances in Geo-Engineering*, Proceedings of the First European Conference on Unsaturated Soils (E-UNSAT 2008), Durham, UK, 2–4 July 2008. Edited by D.G. Toll, C. Augarde, D. Gallipoli, and S. Wheeler. CRC Press, Taylor and Francis Group, Boca Raton, Fla. pp. 653–658.
- Hu, L.B., Hueckel, T., Peron, H., and Laloui, L. 2009. Desiccation shrinkage and its controlling properties: multiphysics. *In Proceedings of the International Conference on Computational Methods for Coupled Problems in Science and Engineering (Coupled Problems 2009)*, Ischia Island, Italy, 8–10 June 2009. Edited by B. Schrefler, E. Oñate, and M. Papadarakakis. CIMNE, Barcelona, Spain.
- Hueckel, T. 1992. Water-mineral interaction in hygro-mechanics of clays exposed to environmental loads: a mixture-theory approach. *Canadian Geotechnical Journal*, **29**(6): 1071–1086. doi:10.1139/t92-124.
- Kleppe, J.H., and Olson, R.E. 1985. Desiccation cracking of soil barrier. *In Hydraulic barriers in soil and rock*. ASTM STP 874. Edited by A.I. Johnson, R.K. Frobel, N.J. Cavalli, and C.B. Pettersson. ASTM International, West Conshohocken, Pa. pp. 263–275. doi:10.1520/STP34583S
- Kodikara, J.K., and Choi, X. 2006. A simplified analytical model for desiccation cracking of clay layers in laboratory tests. *In Unsaturated Soils: Proceedings of the 4th International Conference on Unsaturated Soils*, Carefree, Ariz., 2–6 April 2006. Edited by G.A. Miller, C.E. Zapata, S.L. Houston, and D.G. Fredlund. ASCE Geotechnical Special Publication 147. American Society of Civil Engineers, Reston, Va. Vol. 2. pp. 2558–2569.
- Kodikara, J.K., Barbour, S.L., and Fredlund, D.G. 1999. Changes in clay structure and behaviour due to wetting and drying. *In Proceedings of the Eighth Australia New Zealand Conference on Geomechanics*, Hobart, Tasmania, 15–17 February 1999. Edited by N. Vitharana. Institution of Engineers, Australia. Vol. 1. pp. 179–185.
- Kodikara, J.K., Barbour, S.L., and Fredlund, D.G. 2000. Desiccation cracking of soil layers. *In Proceedings of the First Asian Conference on Unsaturated Soils, Unsaturated Soils for Asia*, Singapore, 18–19 May 2000. Edited by H. Rahardjo, D.G. Toll, and E.C. Leong. A.A. Balkema, Rotterdam, the Netherlands. pp. 693–698.
- Kodikara, J.K., Nahlawi, H., and Bouazza, A. 2004. Modelling of curling in desiccating clay. *Canadian Geotechnical Journal*, **41**(3): 560–566. doi:10.1139/t04-015.
- Konrad, J.M., and Ayad, R. 1997a. Desiccation of a sensitive clay: field experimental observations. *Canadian Geotechnical Journal*, **34**(6): 929–942. doi:10.1139/cgj-34-6-929.
- Konrad, J.M., and Ayad, R. 1997b. An idealized framework for the analysis of cohesive soils undergoing desiccation. *Canadian Geotechnical Journal*, **34**(4): 477–488. doi:10.1139/cgj-34-4-477.
- Kowalski, S.J. 2003. *Thermomechanics of drying processes*. Springer, Berlin.
- Lachenbruch, A.H. 1961. Depth and spacing of tension cracks. *Journal of Geophysical Research*, **66**(12): 4273–4292. doi:10.1029/JZ066i012p04273.
- Lloret, A., Ledesma, A., Rodríguez, R., Sanchez, M.J., Olivella, S., and Suriol, J. 1998. Crack initiation in drying soils. *In Proceedings of the Second International Conference on Unsaturated Soils*, Beijing, China, 27–30 August 1998. International Academic Publishers, Beijing, China. pp. 497–502.
- Micromak. 1998. Winanalyse. Version 1.4 [computer program]. Micromak Service, Berlin, Germany.
- Miller, C.J., Mi, H., and Yesiller, N. 1998. Experimental analysis of desiccation crack propagation in clay liners. *Journal of the American Water Resources Association*, **34**(3): 677–686. doi:10.1111/j.1752-1688.1998.tb00964.x.
- Mitchell, J.K., and Soga, K. 2005. *Fundamentals of soil behavior*. John Wiley & Sons, New York.
- Morris, P.H., Graham, J., and Williams, D.J. 1992. Cracking in drying soils. *Canadian Geotechnical Journal*, **29**(2): 263–277. doi:10.1139/t92-030.
- Nahlawi, H. 2004. Behaviour of a reactive soil during desiccation. M.Sc. thesis, Monash University, Clayton, Australia.
- Nuth, M., and Laloui, L. 2008. Effective stress concept in unsaturated soils: Clarification and validation of a unified framework. *International Journal for Numerical and Analytical Methods in Geomechanics*, **32**(7): 771–801. doi:10.1002/nag.645.
- Or, D., and Tuller, M. 2002. Cavitation during desaturation of porous media under tension. *Water Resources Research*, **38**(5): 19–19-4.
- Peron, H. 2008. Desiccation cracking of soils. Ph.D. thesis, Ecole Polytechnique Fédérale de Lausanne, Lausanne, Switzerland.
- Peron, H., Hueckel, T., and Laloui, L. 2007. An improved volume measurement for determining soil water retention curve. *Geotechnical Testing Journal*, **30**(1): 1–7. doi:10.1520/GTJ100167.
- Peron, H., Delenne, J.Y., Laloui, L., and El Youssofi, M.S. 2009a. Discrete element modelling of drying shrinkage and cracking of soils. *Computers and Geotechnics*, **36**(1–2): 61–69. doi:10.1016/j.compgeo.2008.04.002.
- Peron, H., Laloui, L., Hueckel, T., and Hu, L.B. 2009b. Desiccation cracking of soils. *European Journal of Environmental and Civil Engineering*, **13**: 869–888.
- Rodríguez, R., Sanchez, M., Ledesma, A., and Lloret, A. 2007. Experimental and numerical analysis of desiccation of a mining waste. *Canadian Geotechnical Journal*, **44**(6): 644–658. doi:10.1139/T07-016.
- Scherer, G.W. 1990. Theory of drying. *Journal of the American Ceramic Society*, **73**(1): 3–14. doi:10.1111/j.1151-2916.1990.tb05082.x.
- Scherer, G.W., and Smith, D.M. 1995. Cavitation during drying of

- a gel. *Journal of Non-Crystalline Solids*, **189**(3): 197–211. doi:10.1016/0022-3093(95)00222-7.
- Simpkins, G., Johnson, D.W., Jr., and Fleming, D.A. 1989. Drying behavior of colloidal silica gels. *Journal of the American Ceramic Society*, **72**(10): 1816–1821. doi:10.1111/j.1151-2916.1989.tb05984.x.
- Snyder, V.A., and Miller, R.D. 1985. Tensile strength of unsaturated soils. *Soil Science Society of America Journal*, **49**: 58–65.
- Tarantino, A., and Mongiovi, L. 2001. Experimental procedures and cavitation mechanisms in tensiometer measurements. *Geotechnical and Geological Engineering*, **19**(3–4): 189–210. doi:10.1023/A:1013174129126.
- Terzaghi, K. 1927. Concrete roads – A problem in foundation engineering. *Boston Society of Civil Engineers*, **14**(5): 265–282.
- Terzaghi, K., Peck, R.B., and Mesri, G. 1996. *Soil Mechanics in Engineering Practice*. 3rd ed. John Wiley & Sons, New York.
- UMS GmbH. 2001. UMS T5 Miniature Pressure Pore Transducer, user manual, version 1.8. UMS GmbH, Munich, Germany.
- Van Genuchten, M.T. 1980. A close-form equation for predicting hydraulic conductivity of unsaturated soils. *Soil Science Society of America Journal*, **44**: 892–898.